vector containing glutathione-S-transferase (GST) epitope-tagged anamorsin and selected in the presence of 500 μg/ml G-418 as described previously (Choi et al. 2004). Cells were seeded at a density of 4×10^4 cells or 1×10^6 cells on 25 μg/ml poly-D-lysine (Sigma)-coated aclar film in 4-well culture dishes (NUNC) or P-100 dishes (SPL), respectively. Cells were maintained in an atmosphere of 10% CO_2 for 3 days in Dulbecco's Modified Eagle's Medium (Sigma) supplemented with 10% heat-inactivated fetal bovine serum (Gibco). Cells were subsequently switched to serum-free N2 medium in the presence or absence of the indicated drugs, including 100 μM 6-OHDA (Sigma), 1 μM staurosporine (STS; Sigma), 1.2 mM hydrogen peroxide (Calbiochem), 250 μM cupric chloride (Sigma), 200 μM zinc chloride (Sigma), and 500 μM ferrous chloride (Sigma). If necessary, cells were treated with 5 ng/ml leptomycin B (Sigma) alone or in combination with 100 μM 6-OHDA.

Measurement of ROS

MN9D cells were incubated with or without 100 μM 6-OHDA for 12 h or 1 μM STS for 12 h. Cells were incubated with 3 μM 5-(and-6)-chloromethyl-2′,7′-dichlorodihydrofluorescein diacetate acetyl ester (CM-H2 DCFDA; Molecular Probes) for 30 min at 37°C and washed twice with phosphate-buffered saline (PBS). Stained cells were visualized under an Axio Observer A1 Microscope equipped with epifluorescence and a digital image analyzer (Carl Zeiss).

Stereotaxic surgery and tissue processing

All surgical procedures were conducted in complete accordance with approved animal protocols and guidelines established by Institutional Animal Care and Use Committee (IACUC) at Yonsei University. Male Sprague–Dawley rats (9-weeks-old, 280–300 g; Orient, Suwon, Korea) were housed in a temperature-controlled chamber and maintained at 22 ± 2°C with a 12-h light–dark cycle and free access to food and water. The stereotaxic surgical procedures were performed as previously described with some modifications (Lee et al. 2008). Briefly, rats were anesthetized with chloral hydrate (360 mg/kg, i.p.) and received a unilateral injection of 4 μl 6-OHDA (5 μg/μl in 0.2 mg/ml ascorbate-saline; Sigma) or vehicle-only at a rate of 0.5 μl/min into the right striatum (coordinates, anteroposterior, 0.0; mediolateral, +2.0; dorsoventral, −5.5 from the bregma). Two to three rats were assigned to each condition in one experiment. All injections were performed with a Hamilton syringe equipped with a 30S-gauge beveled needle attached to a syringe pump (KD Scientific, New Hope, PA). After injection, the needle was left in place for an additional 5 min before a slow retraction. For tissue processing, animals were perfused transcardially with a saline solution containing 0.5% sodium nitrate and heparin (1,000 U/ml) prior to fixation with 4% paraformaldehyde (EMS) dissolved in 0.2 M phosphate buffer. Brains were removed and post-fixed overnight in 4% paraformaldehyde at 4°C, incubated in a 30% sucrose solution for 2–3 days at 4°C until they sank, and frozen sections were cut on a sliding microtome into 30-μm-thick coronal sections. Sections were processed for immunohistochemical analyses for tyrosine hydroxylase (TH) alone or in combination with anamorsin as described below.

Immunohistochemistry and cytochemistry

For immunohistochemical localization of TH, tissue sections were permeabilized in 0.2% Triton X-100 (Sigma, T8787) in 0.2 M phosphate buffer at RT for 1 h, blocked in 3% BSA in 0.2 M phosphate buffer at RT for 15 min, and then incubated overnight at 4°C with mouse monoclonal anti-TH (1: 2,000) alone or in combination with rabbit polyclonal anti-anamorsin (1:500) from Labfrontier (Seoul, Korea) which has the same target sequences (anamorsin 2; CRVTGKKPNFEVGSSSQ) as previously described (Shibayama et al. 2004). For immunocytochemical localization of anamorsin following drug treatment, cells were fixed with 4% paraformaldehyde in PBS (Lonza) at RT for 20 min, incubated for 1 h in a blocking buffer containing 0.2% Triton X-100 and 5% normal goat serum (Invitrogen) in PBS, and immunostained with rabbit anti-anamorsin antibody (1:500) or rabbit anti-GST antibody (Santa Cruz; 1:200) overnight at 4°C. After extensive washes with PBS, tissue sections and cells were further incubated at RT for 1 h with appropriate secondary antibodies, including biotinylated goat anti-mouse IgG (Vector Laboratories; 1:1,000), Alexa Fluor 546-conjugated goat anti-mouse IgG, and Alexa Fluor 488-conjugated goat anti-rabbit IgG (Molecular Probes; 1:200). For nuclear staining, tissue sections and cells were incubated at RT for 10 min with Hoechst 33258 (Molecular Probes; 1 μg/ml). Slides were mounted with Vecta Shield mounting medium (Vector Laboratories) and observed under a confocal microscope equipped with an epifluorescence and digital image analyzer (LSM 510 META, Carl Zeiss).

Cellular fractionation and immunoblot analysis

Following drug treatment, MN9D cells were fractionated into cytosolic and nuclear fractions using the digitonin method as previously described with some modifications (Eboue et al. 2003). For tissue lysates, various brain regions and peripheral organs were dissected from each of three Sprague–Dawley rats and solubilized in lysis buffer (50 mM

Tris, pH 8.0, 2 mM EDTA, 1% Triton X-100, and protease inhibitor cocktail) with sonication and centrifuged at 15,000 rpm at 4°C for 20 min. Lysate protein levels were quantified using the Bradford protein assay reagent (Bio-Rad). Equal amounts of soluble proteins were separated on 11.5% or 12.5% sodium dodecyl sulfate (SDS)-polyacrylamide gels and blotted onto a pre-wet polyvinylidene fluoride membrane (Pall Corp). Membranes were then probed with rabbit anti-anamorsin antibody (1:1,000). Both rabbit anti-nucleolin antibody (Santa Cruz; 1:1,000) and goat anti-lamin antibody (Santa Cruz; 1:1,000) were used for nuclear markers, while goat anti-SOD1 antibody (Santa Cruz; 1:1,000) was used for the cytosol marker. For the loading control, rabbit anti-actin antibody (Sigma; 1:3,000) and mouse anti-GAPDH antibody (Millipore; 1:3,000) were used. After extensive washes with Tris-buffered saline containing 0.1% Tween-20 (TBST), cells were incubated with the appropriate secondary antibodies, including horseradish peroxidase-conjugated donkey anti-goat IgG (Abcam; 1:20,000), goat anti-mouse IgG (Santa Cruz; 1:3,000), and goat anti-rabbit IgG (Santa Cruz; 1:3,000). Specific bands were visualized by enhanced chemiluminescence (ECL; Amersham Bioscience).

Results and discussion

Tissue distribution patterns of anamorsin mRNA and protein

A previous study showed that anamorsin is ubiquitously distributed both in fetal and adult tissues as determined by immunohistochemistry (Hao et al. 2006). In the present study, we focused the developmental distribution and expression patterns of anamorsin mRNA in mouse and expression levels of anamorsin protein in adult rat tissues. At first, in situ hybridization using radiolabeled antisense riboprobes (probe #1: 409–909, probe #2:361–670) indicated that

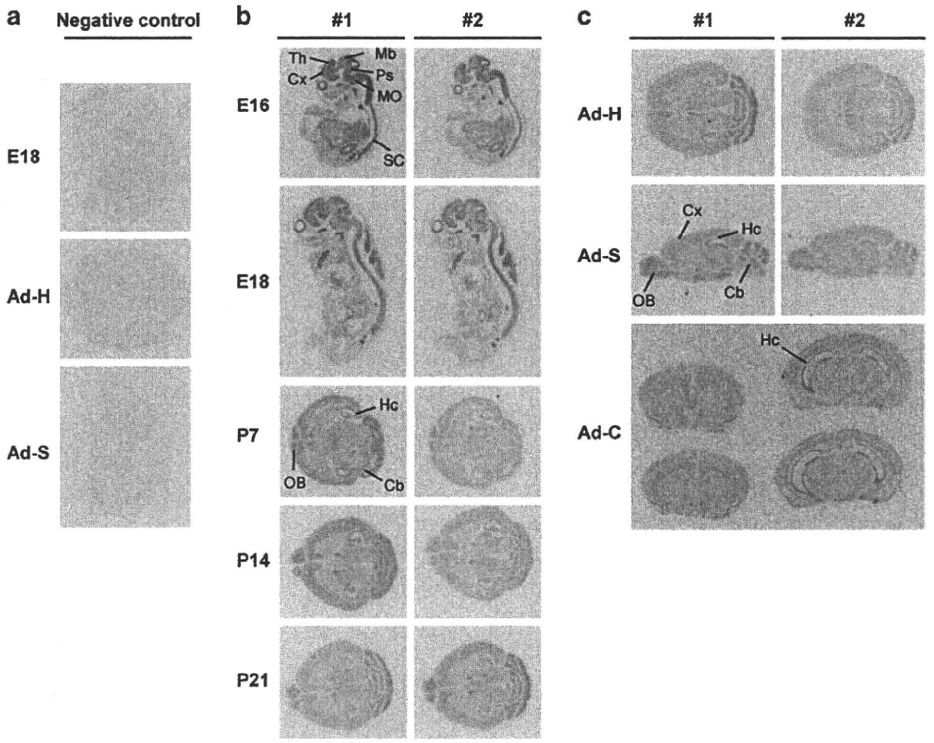

Fig. 1 Anamorsin mRNA expression in mouse tissues. In situ hybridization was performed on various sections of mouse tissues using ^{35}S-labeled riboprobes that target the sequences encompassing 409–909 (probe #1) and 361–670 (probe #2). Tissue sections were hybridized with **a** sense probe or **b**, **c** antisense probe of anamorsin. **a** The specificity of the antisense cRNA probe was determined by the sense version of each riboprobe. Data represent typical negative controls of sense probe #1 obtained from a midsagittal section of the whole body at embryonic day 18 (E18), a horizontal section of adult brain (Ad-H), and a sagittal section of adult brain (Ad-S). Similar negligible signals were also detected using both sense probes from brains at postnatal days 7 (P7), 14 (P14), and 21 (P21), and a coronal section of adult brain (Ad-C; data not shown). **b** From embryonic to postnatal tissue sections, both antisense probes showed a similar expression pattern of anamorsin mRNA in various regions of the central nervous system, including the cerebral cortex (*Cx*), olfactory bulb (*OB*), hippocampus (*Hc*), thalamus (*Th*), midbrain (*Mb*), cerebellum (*Cb*), pons (*Ps*), medulla oblongata (*MO*), and spinal cord (*SC*). **c** Quite similar expression patterns were obtained in three different sectional planes of adult brain. Data are representative images of three independent experiments

the expression of anamorsin mRNA was widespread in various regions of the CNS, although its mRNA expression levels appeared to be higher in embryonic tissues than in neonatal tissues (Fig. 1), including the cerebral cortex, olfactory bulb, hippocampus, thalamus, midbrain, cerebellum, pons, medulla, and spinal cord. On embryonic days 16–18, mRNA expression levels in most regions of the developing CNS were higher than in peripheral organs, including the intestine and heart (Fig. 1b). All of the horizontal, sagittal, and coronal sections of the adult brain demonstrated a widespread expression of anamorsin mRNA (Fig. 1c). Although similar expression patterns of anamorsin mRNA were seen using an antisense probe encompassing nucleotides of 625–927, we did not use this probe for further study due to its weak signal (data not shown). Specificity of the anamorsin mRNA signals was confirmed by comparison with negligible signals on tissue sections hybridized with sense probes (Fig. 1a). For examining protein expression levels of anamorsin in adult rat tissues, we first carried out immunoblot analyses and compared anamorsin expression levels among several peripheral organs, whole brain, and spinal cord. As shown in Fig. 2a, expression levels of anamorsin were much higher in both brain and spinal cord than in most of the peripheral organs including heart, liver, small intestine, kidney, and skeletal muscle. Especially, expression levels of anamorsin in the small intestine, skeletal muscle, and kidney were very low. On the other hand, some of the peripheral organs including the stomach, spleen, and pancreas expressed higher levels of anamorsin. In good accordance with distribution patterns and expression levels of anamorsin mRNA in adult mouse brain, anamorsin protein in rats was widely distributed in many different parts of the brain with similar expression levels (Fig. 2b). It seemed that anamorsin protein was also widely distributed in various parts of the C57BL mouse brain with similar expression levels. These included the cortex, hippocampus, and cerebellum (data not shown). Although it has not been studied, the widespread distribution of anamorsin in fetal, neonatal, and adult brain tissues implies that anamorsin may play important roles in the CNS.

Nuclear translocation of anamorsin following 6-hydroxydoapmine (6-OHDA) treatment

Anamorsin was originally identified as a cytokine-induced anti-apoptotic molecule; its forced expression confers resistance to apoptosis caused by growth factor deprivation in vitro (Shibayama et al. 2004). Subsequent to this early study, underlying protective mechanisms of anamorsin were proposed by others, although they are still largely unclear (Li et al. 2007, 2010; Vernis et al. 2009). With regard to its subcellular localization in normal tissues, Hao et al. (2006) demonstrated that anamorsin was localized in both the cytoplasm and nucleus. Prediction of the subcellular

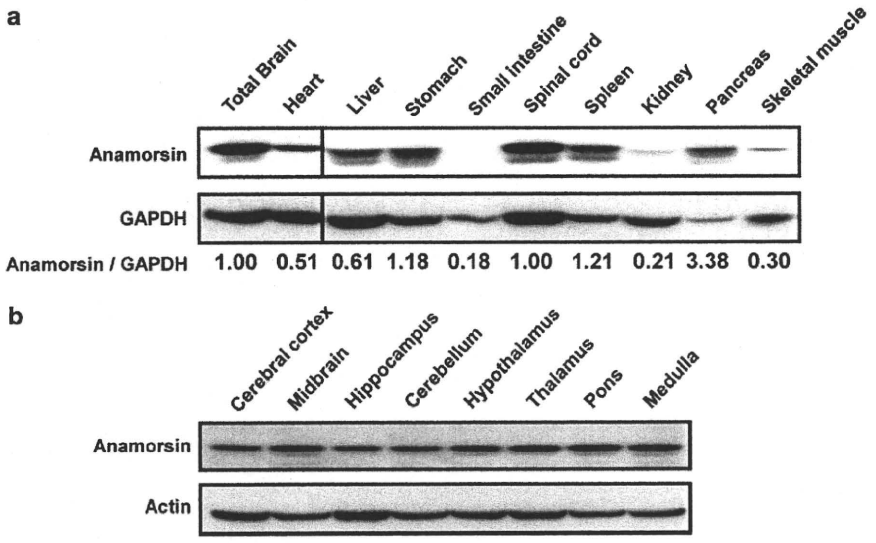

Fig. 2 Expression of anamorsin protein in rat brain. Immunoblot analyses were conducted using tissue lysates obtained from various body regions of the adult rat. Equal amounts of soluble proteins (30 μg) harvested from **a** various regions of the organs and **b** various regions of the brain were subjected to 12.5% sodium dodecyl sulfate-polyacrylamide gel electrophoresis (SDS-PAGE) and immunoblotted with rabbit anti-anamorsin antibody. Both mouse anti-GAPDH and rabbit anti-actin antibodies were used as internal loading controls. The *numbers* under the *blot* represent ratios of anamorsin/GAPDH. Specific bands were visualized by enhanced chemiluminescence after incubation with the horseradish peroxidase-conjugated secondary antibody. While anamorsin was widely expressed in various regions of the brain, relatively higher expression levels of anamorsin were detected in the brain and spinal cord compared those in the heart, liver, small intestine, kidney and skeletal muscle. *Blots* are representative of at least two independent experiments

localization of anamorsin using PSORTII analysis program indicated that anamorsin is mainly localized to the nucleus and, to a lesser extent, in the cytosol, mitochondria, and peroxisome (Li et al. 2010). However, its subcellular localization and potential role in the CNS have not yet been determined. Furthermore, it has not been established whether the subcellular localization of anamorsin can be altered under apoptotic conditions. Therefore, we examined the subcellular localization of anamorsin in dopaminergic neuronal cells both before and after treatment with apoptosis-inducing drugs. Based on our previous studies demonstrating that both a prototypic apoptosis-inducing drug, STS, and a dopaminergic neurotoxin, 6-OHDA, induce caspase-dependent apoptosis in MN9D dopaminergic neuronal cells and in primary cultures of both cortical and dopaminergic neurons (Choi et al. 1999, 2004; Han et al. 2003a, b; Kim et al. 1999; Oh et al. 1997), we conducted an immunocytochemical localization of endogenous anamorsin in MN9D cells treated with either drug. As previously described in our studies and shown in Figs. 3a, 6-OHDA, but not STS, induced a surge of ROS in MN9D cells. As shown in Fig. 3b, anamorsin was primarily localized to the cytosol and, to a lesser extent, to the nucleus prior to drug treatment. However, anamorsin was translocated into the nucleus following 6-OHDA treatment. Intriguingly, STS did not cause any discernible nuclear translocation of anamorsin, suggesting that it is a ROS-dependent event. Since the molecular weight of anamorsin is approximately 33 kDa, it may passively diffuse from the cytosol to the nucleus through the nuclear pore complex (Capelson and Hetzer 2009; Weis 2007). To eliminate this possibility, we constructed a vector containing anamorsin with a C-terminal glutathione-S-transferase (GST) tag to increase the theoretical size of anamorsin and establish a stable cell line

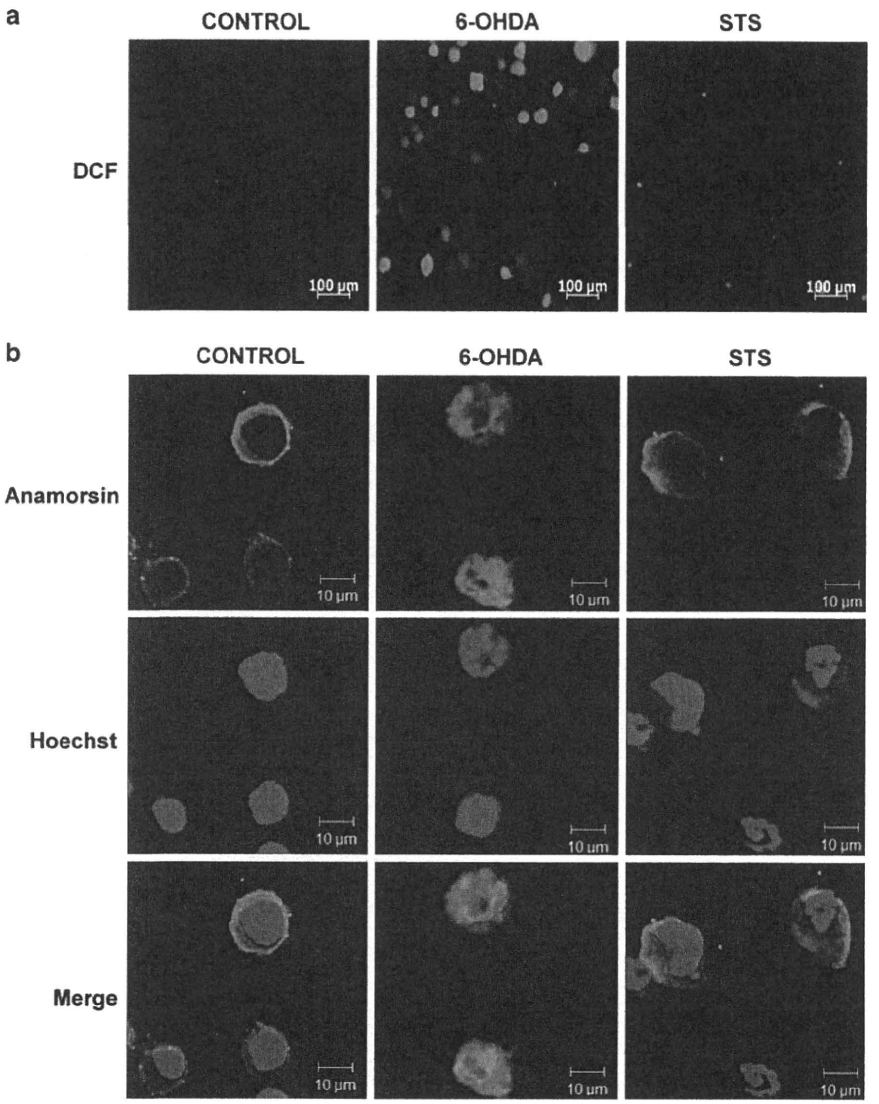

Fig. 3 Nuclear translocation of anamorsin in MN9D cells following 6-hydroxydopamine (6-OHDA) treatment. **a** Measurement of levels of reactive oxygen species was carried out using a hydrogen peroxide-sensitive fluorescent probe, CM-H2 DCFDA (DCF) in MN9D dopaminergic neuronal cells following treatment with or without 100 μM 6-OHDA and 1 μM staurosporine (STS) for 12 h. Increased DCF-positive cells were detected in wells treated with 6-OHDA but not in wells treated with STS. **b** Immunocytochemical localization of anamosin in drug-treated MN9D cells was performed. Twelve hours after drug treatment, cells were fixed in 4% paraformaldehyde and subsequently incubated with rabbit anti-anamorsin antibody followed by incubation with Alexa 488-conjugated goat anti-rabbit IgG antibody. Nuclear staining was done with Hoechst dye. Confocal photomicrographs are representative of at least three independent experiments. *Merge views* indicate nuclear translocation of anamorsin following 6-OHDA but not STS treatment. We adjusted the background signals by using MetaMorph program

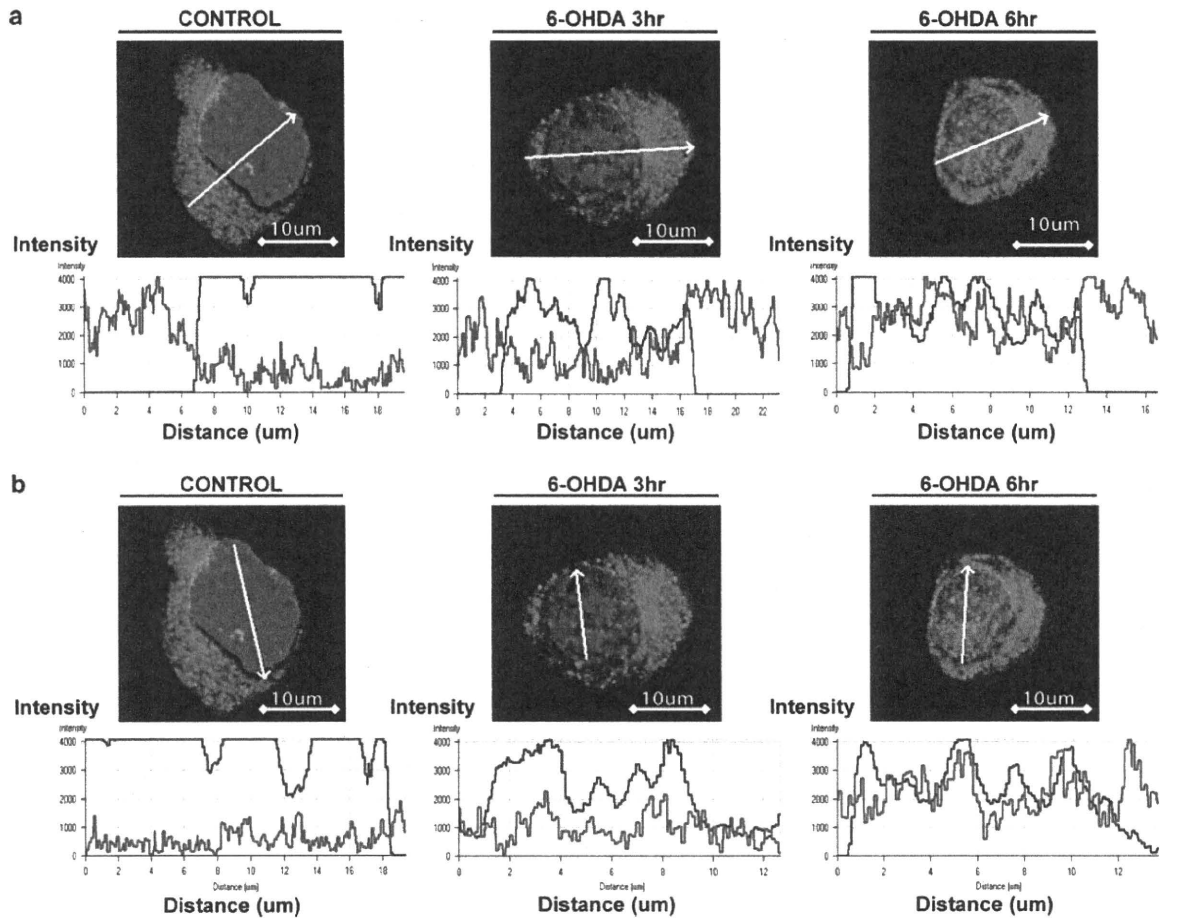

Fig. 4 Nuclear translocation of glutathione-S-transferase (GST)-tagged anamorsin in MN9D cells following 6-OHDA treatment. MN9D cells stably expressing GST-tagged anamorsin were established and treated with or without 100 μM 6-OHDA for the indicated times. Following drug treatment, cells were subjected to immunocytochemical analyses using rabbit anti-GST antibody followed by incubation with Alexa 488-conjugated goat anti-rabbit IgG. Nuclear staining was done with Hoechst dye. The signals observed by confocal microscopy were analyzed with a digital image analyzer for **a** the entire cell or **b** nucleus only. *Graphs* below micrographs represent the intensities of the anamorsin (*green lines*) and nuclear (*blue lines*) signals from the cross-sectional area marked by a white arrow. The time-dependent nuclear translocation of GST-tagged anamorsin was observed among 25 randomly selected 6-OHDA-treated cells from three independent experiments

in MN9D cells. As shown in Fig. 4, both the confocal micrographs and their analyses indicate that 6-OHDA treatment leads to the nuclear translocation of the GST-fused anamorsin in a time-dependent manner, suggesting an active transport process.

To further validate the immunocytochemical data and to indirectly evaluate whether nuclear transport of anamorsin can be regulated by the nuclear transport complex, immunoblot analyses were performed using soluble proteins harvested from the nuclear fractions following the indicated drug treatment. Consistent with immunocytochemical localization analyses (e.g., Figs. 3, 4), we observed that 6-OHDA treatment resulted in a time-dependent translocation of anamorsin into the nuclear fraction (Fig. 5a, right panel). In contrast, STS did not cause any discernible changes at any time. Leptomycin B (LMB), initially discovered as an anti-fungal antibiotic, is a secondary metabolite produced by *Streptomyces* (Hamamoto et al. 1983). Among its many other proposed functions, LMB was demonstrated to be a potent and specific nuclear export inhibitor (Ferraiuolo et al. 2004; Katayama et al. 2010; Neary and Pastorino 2010; Nishi et al. 1994). LMB can alkylate and inhibit chromosomal region maintenance (CRM1)/exportin 1, which is critical for the nuclear export of RNA and proteins containing a nuclear export sequence. We, therefore, conducted immunoblot analyses to determine whether LMB could regulate the nuclear translocation of anamorsin under both normal and 6-OHDA treatment conditions. As shown in Fig. 5b (right panel), higher levels of anamorsin accumulated in the nuclear fraction of MN9D cells treated with

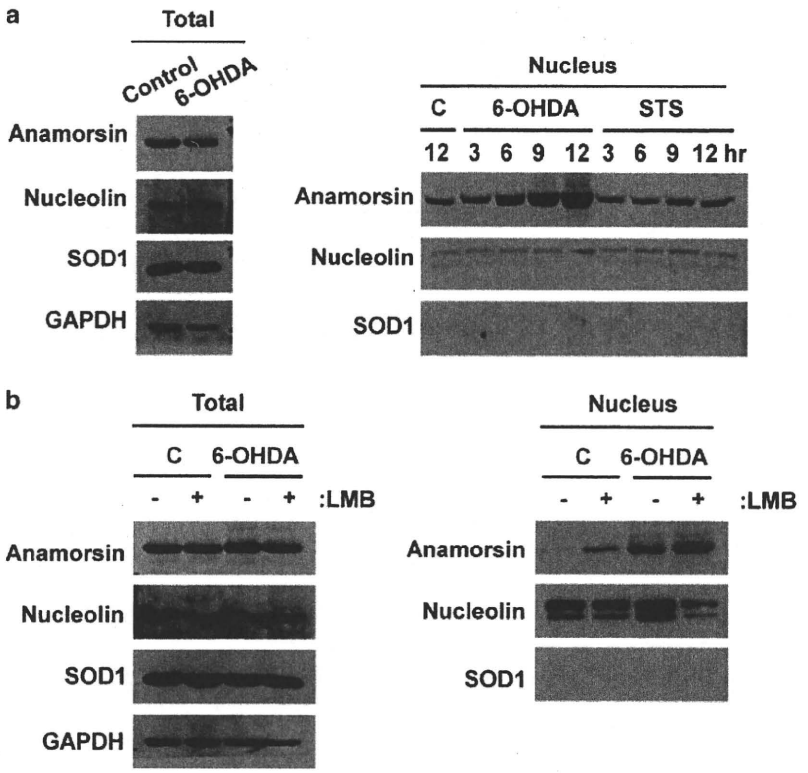

Fig. 5 Immunoblot analyses of anamorsin in nuclear fractions of MN9D cells following drug treatment. **a** MN9D cells were treated with or without 100 μM 6-OHDA and 1 μM STS for the indicated times. Equal amounts of the total and nuclear fraction samples (30 μg) were subjected to 12.5 and 11.5% SDS-PAGE, respectively, and subsequently immunoblotted with rabbit anti-anamorsin antibody. Rabbit anti-nucleolin antibody and goat anti-SOD1 antibody were used for nuclear and cytosolic fraction markers, respectively. A time-dependent accumulation of anamorsin in the nuclear fraction was only observed following 6-OHDA treatment but not STS treatment. **b** MN9D cells were treated for the indicated times with 5 ng/ml leptomycin B (LMB) alone or in combination with 100 μM 6-OHDA. Treatment with LMB alone or co-treatment of LMB and 6-OHDA led to increased levels of anamorsin in the nuclear fraction while total level of anamorsin was not increased. *Blots* are representative of three independent experiments

LMB. In MN9D cells treated with 6-OHDA, co-treatment with LMB accelerated the rate of the 6-OHDA-induced nuclear accumulation of anamorsin. We observed that LMB, either alone or in combination with 6-OHDA, itself did not lead to an increase in total anamorsin levels in MN9D cells (Fig. 5, left panel); our data, therefore, suggest that anamorsin may be constantly trafficking into and out of the nucleus and that 6-OHDA disrupts this dynamic, resulting in the nuclear accumulation of anamorsin.

To confirm that this phenomenon is confined only to MN9D cells, we conducted immunohistochemical localization analysis of anamorsin using a unilaterally lesioned rat brain model. As previously demonstrated (Lee et al. 2008), stereotaxic injection of 6-OHDA into the striatum resulted in a loss of tyrosine hydroxylase (TH)-positive neurons on the ipsilateral side of the midbrain (Fig. 6a). Counting of the cresyl violet-positive cells ensured that the loss of TH-positive neurons by 6-OHDA injection was not simply due to a loss of TH immunoreactivity (data not shown; also see Lee et al. 2008). In the contralateral side of 6-OHDA-lesioned (data not shown) or vehicle-injected midbrain sections, colocalization analyses for TH and anamorsin indicated that anamorsin was largely present in the cytosol under normal conditions and its nuclear translocation was found in some TH-positive and TH-negative cells following 6-OHDA injection (Fig. 6b). In primary cultures of dopaminergic neurons, equal amounts of anamorsin were present in the cytosol and nucleus under normal conditions (data not shown). Nevertheless, treatment with 6-OHDA resulted in higher levels of nuclear anamorsin in TH-positive and TH-negative cells (data not shown), confirming that 6-OHDA triggers the nuclear accumulation of anamorsin in all dopaminergic neurons tested. This was quite contrary to the previous finding by Hao et al. (2006) demonstrating that anamorsin is located in the nucleus and accumulated in the nucleoli under normal conditions. It is not clear at present whether this discrepancy is simply due to the different cell types studied or different types of fixative utilized for the immunostaining (Bjorkoy et al. 2009). Considering our preliminary observation that

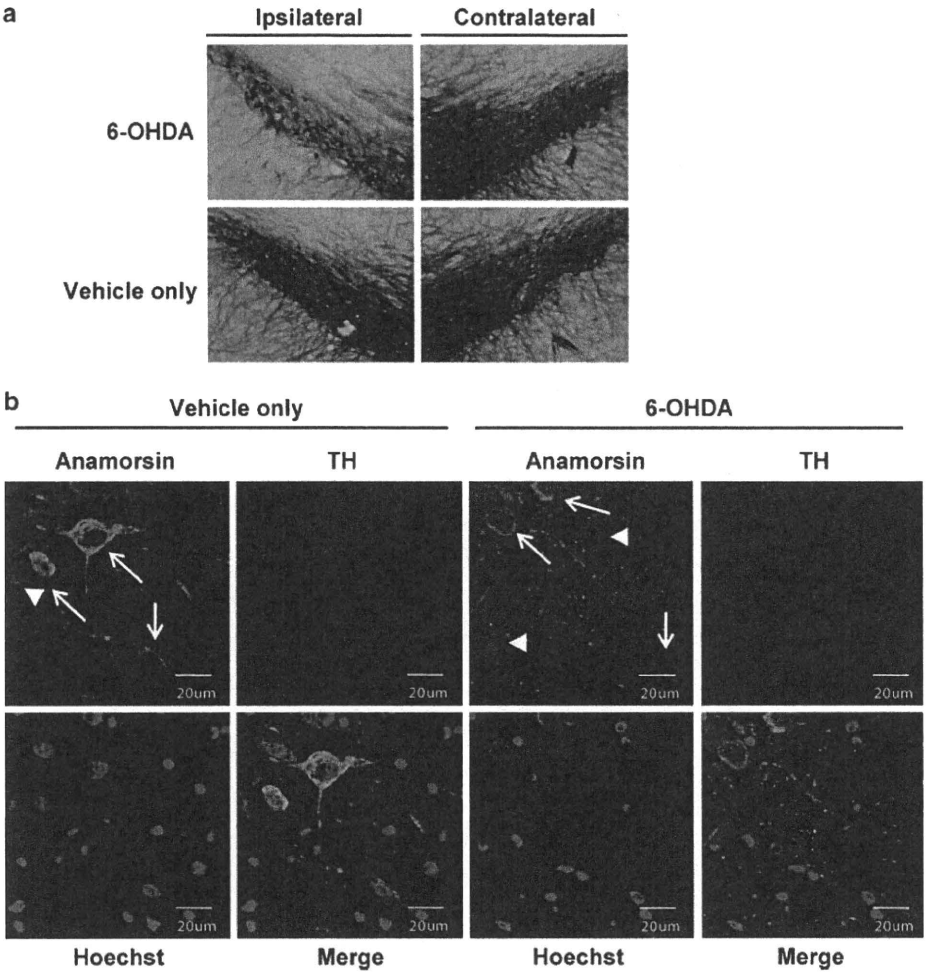

Fig. 6 Nuclear translocation of anamorsin in 6-OHDA-injected rat brain. Rats received a unilateral injection of 4 μl (total 20 μg) 6-OHDA in ascorbate-saline or vehicle-only at a rate of 0.5 μl/min into the right striatum. Seven days after stereotaxic injection, the brains were processed for immunohistochemical localization of **a** tyrosine hydroxylase (TH) alone or **b** in combination with anamorsin in the midbrain sections. **a** Ipsilateral and contralateral sides of the coronal sections of the midbrain were obtained from vehicle-only or 6-OHDA-injected rats and immunostained with mouse anti-TH antibody followed by biotinylated goat anti-mouse IgG. The apparent loss of TH-positive neurons was detected only in the ipsilateral side of the 6-OHDA-injected rat midbrain. **b** Both ipsilateral sides of vehicle-only or 6-OHDA-injected rat brain sections were processed for double immunofluorescent localization using mouse anti-TH and rabbit anti-anamorsin antibodies followed by incubation with Alexa 568-conjugated goat anti-mouse IgG and Alexa 488-conjugated goat anti-rabbit IgG. Nuclear staining was performed with Hoechst dye. *Arrows* indicate TH-positive neurons with anamorsin, while arrowheads point to TH-negative cells with anamorsin in the ipsilateral side of vehicle-only and 6-OHDA-injected rat brain. We adjusted the background signals by using MetaMorph program

anamorsin was primarily localized to the nuclei of human embryonic kidney (HEK293) cells and human neuoblastoma (SH-SY5Y) cells, our data raise the possibility that the proportion of nuclear anamorsin may be regulated by cell origin and context.

Dopaminergic neurons in the substantia nigra pars compacta are vulnerable to neurodegeneration because of high levels of ROS (Ben-Shachar et al. 1991; Fahn and Cohen 1992; Jenner 1998; Miller et al. 2009). Given the biochemical changes reminiscent of those occurring in patients with PD, several neurotoxins, including 6-OHDA, have been widely used to establish experimental PD models (Beal 2001; Dauer and Przedborski 2003). Our previous studies (Choi et al. 1999; Glinka et al. 1997; Han et al. 2003a) indicate that cytotoxicity rendered by 6-OHDA is primarily due to high ROS levels in the dopaminergic neurons. To determine the specificity of the 6-OHDA-triggered nuclear translocation of anamorsin, we treated MN9D cells with other well-known pro-oxidants and performed immunoblot analyses using both the cytosolic and nuclear fractions. Since levels of anamorsin were much higher in the cytosol than in the nucleus of the

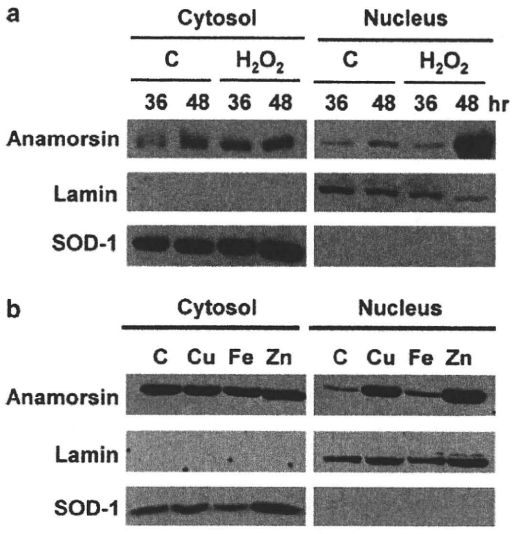

Fig. 7 Nuclear translocation of anamorsin in MN9D cells following reactive oxygen species (ROS)-inducing drugs. **a** MN9D cells treated with 1.2 mM hydrogen peroxide for the indicated times were subjected to cellular fractionation. Equal amounts (3 μg) of cytosolic and nuclear (30 μg) fractionated protein samples were separated by 11.5% SDS-PAGE and immunoblotted with rabbit anti-anamorsin antibody. Goat anti-lamin and goat anti-SOD1 antibodies were used for nuclear and cytosolic markers, respectively. **b** MN9D cells treated for 10 h with 250 μM cupric chloride (Cu), 500 μM ferrous chloride (Fe), or 200 μM zinc chloride (Zn) were subjected to cellular fractionation. Equal amounts of cytosolic (3 μg) or nuclear proteins (30 μg) were subjected to 11.5% SDS-PAGE. Subsequent immunoblot analyses were conducted as described above. All of the ROS-inducing drugs promoted the nuclear translocation of anamorsin in MN9D cells. *Blots* are representative of at least three independent experiments

MN9D cells, one-tenth of cytosolic proteins were loaded to avoid the saturation of the signal during immunoblot analyses. Therefore, 3 μg of the cytosolic fraction and 30 μg of the nuclear fraction were utilized for control and drug-treated groups. Based on the present data indicating that 6-OHDA triggers an increase in hydrogen peroxide-sensitive DCF-positive cells (Fig. 3a), MN9D cells were first treated with 1.2 mM hydrogen peroxide for the indicated times. Immunoblot analyses demonstrated that external application of hydrogen peroxide promoted dramatic nuclear translocation of anamorsin at 48 h (>~10-fold over the control; Fig. 7a). Lower concentrations than 1 mM hydrogen peroxide and shorter incubation times than 36 h did not cause any discernible changes. However, treatment of cells with 2.4 mM hydrogen peroxide promoted a slight but significant nuclear translocation of anamorsin as early as 30 min after treatment (1.4–1.6-fold over the control). Trace metal elements, including cupric chloride, ferrous chloride, and zinc chloride, are known to induce high levels of various ROS, including hydrogen peroxide (Mladenka et al. 2006; Qian et al. 2005; Sensi et al. 2009). Indeed, treatment of MN9D cells with each of these trace metal elements for 10 h triggered the dramatic appearance of hydrogen peroxide-sensitive and DCF-positive cells (data not shown). The staining intensity of the DCF-positive cells was much greater in cells treated with cupric chloride or zinc chloride compared to ferrous chloride (data not shown). As shown in Fig. 7b, the nuclear translocation of anamorsin was obvious in MN9D cells treated with either cupric chloride or zinc chloride for 10 h. However, much lower amounts of nuclear anamorsin were translocated into the nucleus following ferrous chloride treatment. Considering that virtually no signs of nuclear translocation of anamorsin were found in the STS-treated cells, our present data suggest that the translocation of anamorsin into the nucleus is primarily controlled by ROS.

To our knowledge, we are the first to demonstrate the (sub)cellular distribution and expression of anamorsin both under normal and drug-induced pathophysiological conditions in dopaminergic neurons in vivo. We propose that the nuclear translocation of anamorsin is largely dependent on the presence of ROS in dopaminergic neurons. This hypothesis is in good accordance with previous studies that demonstrate hydrogen peroxide initiates the nuclear translocation of proteins such as p53 and FOXO (Jang et al. 2007; Uberti et al. 1999). Intriguingly, our preliminary study using immunoprecipitation followed by mass spectral analyses suggests that anamorsin may bind to many critical molecules in the nucleus, including double-stranded DNA, ribosomal proteins, and histones (data not shown), implying that anamorsin may play an essential role in the transcriptional regulation of critical molecules associated with neuronal cell survival and death. Indeed previous report (Shibayama et al., 2004) shows that anamorsin −/− mouse embryos began to die between E12.5 and E14.5. In the end, all anamorsin −/− mice died at birth. In that article, they described that this phenomena related to the level of anti-apoptotic molecules like JAK2 and Bcl-XL. In anamorsin −/− mice, mRNA level of Jak2 and Bcl-XL decrease compare to anamorsin +/+ mice. Based on this data, we think that nuclear anamorsin promotes transcription of anti-apoptotic molecules like Jak2 and Bcl-XL. Therefore, nuclear translocation of anamorsin promotes its anti-apoptotic effect as a transcriptional regulator. Although the potential roles for nuclear anamorsin were recently proposed (Li et al. 2010), more direct evidence remains to be demonstrated. Similarly, other critical questions regarding how anamorsin is translocated into the nucleus and what the potential target molecules are in the nucleus also remain to be determined. With these and many other related questions in mind, further studies examining the molecular and cellular events associated with the role of anamorsin in different subcellular regions may reveal its definitive role in the CNS and, specifically, in neurodegeneration.

Acknowledgments The authors thank Dr. A. Heller for allowing us to use the MN9D cell line. We also greatly appreciate critical suggestions made by Dr. Moussa B.H. Youdim. We would like to dedicate much of our work to Dr. Youdim on his 70th birthday. This work was supported by a grant from Ministry of Health and Welfare (A090063), and, in part, by the Brain Research Center, World Class University (WCU, R33-2208-10014) and KOSEF through SRC (R11-2008-036).

References

Basso M, Giraudo S, Corpillo D, Bergamasco B, Lopiano L, Fasano M (2004) Proteome analysis of human substantia nigra in Parkinson's disease. Proteomics 4(12):3943–3952

Beal MF (2001) Experimental models of Parkinson's disease. Nat Rev Neurosci 2(5):325–334

Ben-Shachar D, Eshel G, Finberg JP, Youdim MB (1991) The iron chelator desferrioxamine (Desferal) retards 6-hydroxydopamine-induced degeneration of nigrostriatal dopamine neurons. J Neurochem 56(4):1441–1444

Bjorkoy G, Lamark T, Pankiv S, Overvatn A, Brech A, Johansen T (2009) Monitoring autophagic degradation of p62/SQSTM1. Methods Enzymol 452:181–197

Blennow K, Hampel H, Weiner M, Zetterberg H (2010) Cerebrospinal fluid and plasma biomarkers in Alzheimer disease. Nat Rev Neurol 6(3):131–144

Capelson M, Hetzer MW (2009) The role of nuclear pores in gene regulation, development and disease. EMBO Rep 10(7):697–705

Choi HK, Won LA, Kontur PJ, Hammond DN, Fox AP, Wainer BH, Hoffmann PC, Heller A (1991) Immortalization of embryonic mesencephalic dopaminergic neurons by somatic cell fusion. Brain Res 552(1):67–76

Choi WS, Yoon SY, Oh TH, Choi EJ, O'Malley KL, Oh YJ (1999) Two distinct mechanisms are involved in 6-hydroxydopamine- and MPP+-induced dopaminergic neuronal cell death: role of caspases, ROS, and JNK. J Neurosci Res 57(1):86–94

Choi WS, Eom DS, Han BS, Kim WK, Han BH, Choi EJ, Oh TH, Markelonis GJ, Cho JW, Oh YJ (2004) Phosphorylation of p38 MAPK induced by oxidative stress is linked to activation of both caspase-8- and -9-mediated apoptotic pathways in dopaminergic neurons. J Biol Chem 279(19):20451–20460

Dauer W, Przedborski S (2003) Parkinson's disease: mechanisms and models. Neuron 39(6):889–909

Eboue D, Auger R, Angiari C, Le Doan T, Tenu JP (2003) Use of a simple fractionation method to evaluate binding, internalization and intracellular distribution of oligonucleotides in vascular smooth muscle cells. Arch Physiol Biochem 111(3):265–272

Fahn S, Cohen G (1992) The oxidant stress hypothesis in Parkinson's disease: evidence supporting it. Ann Neurol 32(6):804–812

Ferraiuolo MA, Lee CS, Ler LW, Hsu JL, Costa-Mattioli M, Luo MJ, Reed R, Sonenberg N (2004) A nuclear translation-like factor eIF4AIII is recruited to the mRNA during splicing and functions in nonsense-mediated decay. Proc Natl Acad Sci USA 101(12):4118–4123

Glinka Y, Gassen M, Youdim MB (1997) Mechanism of 6-hydroxydopamine neurotoxicity. J Neural Transm Suppl 50:55–66

Hamamoto T, Gunji S, Tsuji H, Beppu T (1983) Leptomycins A and B, new antifungal antibiotics. I. Taxonomy of the producing strain and their fermentation, purification and characterization. J Antibiot (Tokyo) 36(6):639–645

Han BS, Hong HS, Choi WS, Markelonis GJ, Oh TH, Oh YJ (2003a) Caspase-dependent and -independent cell death pathways in primary cultures of mesencephalic dopaminergic neurons after neurotoxin treatment. J Neurosci 23(12):5069–5078

Han BS, Noh JS, Gwag BJ, Oh YJ (2003b) A distinct death mechanism is induced by 1-methyl-4-phenylpyridinium or by 6-hydroxydopamine in cultured rat cortical neurons: degradation and dephosphorylation of tau. Neurosci Lett 341(2):99–102

Hao Z, Li X, Qiao T, Zhang J, Shao X, Fan D (2006) Distribution of CIAPIN1 in normal fetal and adult human tissues. J Histochem Cytochem 54(4):417–426

Jang SW, Yang SJ, Srinivasan S, Ye K (2007) Akt phosphorylates MstI and prevents its proteolytic activation, blocking FOXO3 phosphorylation and nuclear translocation. J Biol Chem 282(42):30836–30844

Jenner P (1998) Oxidative mechanisms in nigral cell death in Parkinson's disease. Mov Disord 13(Suppl 1):24–34

Jin J, Hulette C, Wang Y, Zhang T, Pan C, Wadhwa R, Zhang J (2006) Proteomic identification of a stress protein, mortalin/mthsp70/GRP75: relevance to Parkinson disease. Mol Cell Proteomics 5(7):1193–1204

Katayama R, Ishioka T, Takada S, Takada R, Fujita N, Tsuruo T, Naito M (2010) Modulation of Wnt signaling by the nuclear localization of cellular FLIP-L. J Cell Sci 123(Pt 1):23–28

Kim JE, Oh JH, Choi WS, Chang II, Sohn S, Krajewski S, Reed JC, O'Malley KL, Oh YJ (1999) Sequential cleavage of poly(ADP-ribose)polymerase and appearance of a small Bax-immunoreactive protein are blocked by Bcl-X(L) and caspase inhibitors during staurosporine-induced dopaminergic neuronal apoptosis. J Neurochem 72(6):2456–2463

Klein C, Schlossmacher MG (2006) The genetics of Parkinson disease: implications for neurological care. Nat Clin Pract Neurol 2(3):136–146

Lee YM, Park SH, Chung KC, Oh YJ (2003) Proteomic analysis reveals upregulation of calreticulin in murine dopaminergic neuronal cells after treatment with 6-hydroxydopamine. Neurosci Lett 352(1):17–20

Lee YM, Park SH, Shin DI, Hwang JY, Park B, Park YJ, Lee TH, Chae HZ, Jin BK, Oh TH et al (2008) Oxidative modification of peroxiredoxin is associated with drug-induced apoptotic signaling in experimental models of Parkinson disease. J Biol Chem 283(15):9986–9998

Levine B, Kroemer G (2008) Autophagy in the pathogenesis of disease. Cell 132(1):27–42

Li X, Hong L, Zhao Y, Jin H, Fan R, Du R, Xia L, Luo G, Fan D (2007) A new apoptosis inhibitor, CIAPIN1 (cytokine-induced apoptosis inhibitor 1), mediates multidrug resistance in leukemia cells by regulating MDR-1, Bcl-2, and Bax. Biochem Cell Biol 85(6):741–750

Li X, Wu K, and Fan D (2010) CIAPIN1 as a therapeutic target in cancer. Expert Opin Ther Targets 14(6):603–610

Licker V, Kovari E, Hochstrasser DF, Burkhard PR (2009) Proteomics in human Parkinson's disease research. J Proteomics 73(1):10–29

Mattson MP (2000) Apoptosis in neurodegenerative disorders. Nat Rev Mol Cell Biol 1(2):120–129

Miller RL, James-Kracke M, Sun GY, Sun AY (2009) Oxidative and inflammatory pathways in Parkinson's disease. Neurochem Res 34(1):55–65

Mladenka P, Simunek T, Hubl M, Hrdina R (2006) The role of reactive oxygen and nitrogen species in cellular iron metabolism. Free Radic Res 40(3):263–272

Moore DJ, West AB, Dawson VL, Dawson TM (2005) Molecular pathophysiology of Parkinson's disease. Annu Rev Neurosci 28:57–87

Neary CL, and Pastorino JG (2010) Nucleocytoplasmic shuttling of hexokinase II in a cancer cell. Biochem Biophys Res Commun 394(4):1075–81

Nishi K, Yoshida M, Fujiwara D, Nishikawa M, Horinouchi S, Beppu T (1994) Leptomycin B targets a regulatory cascade of crm1,

a fission yeast nuclear protein, involved in control of higher order chromosome structure and gene expression. J Biol Chem 269(9): 6320–6324

Oh YJ, Uhland-Smith A, Kim JE, O'Malley KL (1997) Regions outside of the Bcl-2 homology domains, BH1 and BH2 protect a dopaminergic neuronal cell line from staurosporine-induced cell death. Brain Res Mol Brain Res 51(1–2):133–142

Park SA, Park HW, Kim NH, Kim YH, Kwak MJ, Shin JS, Kim CW (2010) Effects of Tau on the activity of triose phosphate isomerase (TPI) in brain cells. Neurochem Int 56(8):886–892

Pienaar IS, Daniels WM, Gotz J (2008) Neuroproteomics as a promising tool in Parkinson's disease research. J Neural Transm 115(10):1413–1430

Qian Y, Zheng Y, Abraham L, Ramos KS, Tiffany-Castiglioni E (2005) Differential profiles of copper-induced ROS generation in human neuroblastoma and astrocytoma cells. Brain Res Mol Brain Res 134(2):323–332

Rubinsztein DC, Gestwicki JE, Murphy LO, Klionsky DJ (2007) Potential therapeutic applications of autophagy. Nat Rev Drug Discov 6(4):304–312

Sensi SL, Paoletti P, Bush AI, Sekler I (2009) Zinc in the physiology and pathology of the CNS. Nat Rev Neurosci 10(11):780–791

Shibayama H, Takai E, Matsumura I, Kouno M, Morii E, Kitamura Y, Takeda J, Kanakura Y (2004) Identification of a cytokine-induced antiapoptotic molecule anamorsin essential for definitive hematopoiesis. J Exp Med 199(4):581–592

Spillantini MG, Schmidt ML, Lee VM, Trojanowski JQ, Jakes R, Goedert M (1997) Alpha-synuclein in Lewy bodies. Nature 388(6645):839–840

Uberti D, Yavin E, Gil S, Ayasola KR, Goldfinger N, Rotter V (1999) Hydrogen peroxide induces nuclear translocation of p53 and apoptosis in cells of oligodendroglia origin. Brain Res Mol Brain Res 65(2):167–175

Van Laar VS, Dukes AA, Cascio M, Hastings TG (2008) Proteomic analysis of rat brain mitochondria following exposure to dopamine quinone: implications for Parkinson disease. Neurobiol Dis 29(3):477–489

Vernis L, Facca C, Delagoutte E, Soler N, Chanet R, Guiard B, Faye G, Baldacci G (2009) A newly identified essential complex, Dre2-Tah18, controls mitochondria integrity and cell death after oxidative stress in yeast. PLoS One 4(2):e4376

Weis K (2007) The nuclear pore complex: oily spaghetti or gummy bear? Cell 130(3):405–407

Zhang J, Sokal I, Peskind ER, Quinn JF, Jankovic J, Kenney C, Chung KA, Millard SP, Nutt JG, Montine TJ (2008) CSF multianalyte profile distinguishes Alzheimer and Parkinson diseases. Am J Clin Pathol 129(4):526–529

OPEN ACCESS Freely available online

PLoS one

The Density of CD10 Corresponds to Commitment and Progression in the Human B Lymphoid Lineage

Michiko Ichii[1], Kenji Oritani[2], Takafumi Yokota[2], Qingzhao Zhang[1], Karla P. Garrett[1], Yuzuru Kanakura[2], Paul W. Kincade[1]*

1 Immunobiology and Cancer Program, Oklahoma Medical Research Foundation, Oklahoma City, Oklahoma, United States of America, **2** Department of Hematology and Oncology, Osaka University Graduate School of Medicine, Osaka, Japan

Abstract

Background: Requirements for human B lymphopoiesis are still poorly understood, and that has hampered investigation of differentiation events. For example, there are few cell surface antigens that can be used as milestones of lineage progression. The CD10 ectoenzyme is one such marker and has been used to define CLP, but we found substantial tissue specific variations in CD10 levels, and there was no information about how that corresponded to differentiation options.

Methodology/Principal Findings: The aim of the present study was to use recently developed culture methods to assess the nature and differentiation potential of progenitors sorted according to CD10 density from umbilical cord blood (CB), adult bone marrow (BM) or G-CSF mobilized peripheral blood (PB). Many $CD34^+$ cells in BM express high levels of CD10, while low or low/negative CD10 densities were found on $CD34^+$ cells in CB or G-CSF mobilized PB, respectively. The relative abundance of $CD10^{Lo}$ versus $CD10^{Hi}$ cells only accounts for some CB versus BM differences. Almost all of the $CD34^+$ $CD10^{Hi}$ cells expressed CD19 and lymphocyte transcription factors and corresponded to loss of myeloid potential. A high degree of immunoglobulin D_H-J_H gene rearrangements was characteristic only of the $CD10^{Hi}$ subset. In contrast, the $CD34^+$ $CD10^{Lo}$ progenitors efficiently produced plasmacytoid and conventional dendritic cells as well as myeloid cells. These findings suggest a positive correlation between CD10 density and degree of differentiation. Although freshly isolated $CD34^+$ $CD10^{Hi}$ cells were in cycle, those from CB or BM expanded poorly in culture, suggesting regulators of populations remain to be discovered.

Conclusions/Significance: Steps in human B lymphopoiesis have not been sufficiently studied, and we now show that increased CD10 expression corresponds to differentiation potential and stage. $CD34^+$ $CD10^{Hi}$ progenitors are obviously in the B lineage but may have progressed beyond the point where they can be expanded in culture.

Citation: Ichii M, Oritani K, Yokota T, Zhang Q, Garrett KP, et al. (2010) The Density of CD10 Corresponds to Commitment and Progression in the Human B Lymphoid Lineage. PLoS ONE 5(9): e12954. doi:10.1371/journal.pone.0012954

Editor: Derya Unutmaz, New York University, United States of America

Received June 6, 2010; **Accepted** August 16, 2010; **Published** September 23, 2010

Funding: This work was supported by grant AI020069 (P.W.K.) from the National Institutes of Health. The funders had no role in study design, data collection and analysis, decision to publish, or preparation of the manuscript. P.W.K. holds the William H. and Rita Bell Endowed Chair in Biomedical Research.

Competing Interests: The authors have declared that no competing interests exist.

* E-mail: kincade@omrf.ouhsc.edu

Introduction

Common lymphoid progenitors (CLP) were originally defined in mice as lineage marker negative, IL-7Rα$^+$, Sca-1$^+$, c-Kit^{Lo} cells that appeared to be largely restricted to the production of B, T and NK cells [1]. The original CLP subset has been subdivided and re-defined in multiple ways, and the potential of these cells to produce small numbers of non-lymphoid cells is still debated [2–7]. Moreover, a picture is emerging of asynchronous expression of lymphoid genes and markers, with gradual restriction of differentiation options [8,9].

Although the CD10 ectoenzyme is not expressed on murine progenitors, it has been used in the definition of human CLP [10–12]. The current consensus is that CD10 is expressed on early, pro-, and pre- B cells while levels are down-regulated after development to mature B cells. Other markers exploited in studies of human but not murine CLP include CD45RA, CD7 and CD38 [13–15]. In addition, multiple differentiation pathways can result in production of similar cells such as T and B lymphocytes [16–18]. There are additional reasons comparisons between murine and human lymphoid progenitors are difficult. For example, IL-7 is not essential for human B lymphopoiesis, and no factors have been discovered that support efficient B lymphoid lineage progression in culture [19]. For these and other reasons, results obtained in studies conducted with bone marrow from young adult mice are not readily comparable to those using human umbilical cord blood (CB), adult bone marrow (BM) or G-CSF mobilized peripheral blood (G-PB).

Allogeneic hematopoietic stem cell transplantation is a curative treatment for patients with hematopoietic malignancies and marrow failure syndrome [20–22]. However, the composition of the donor inoculum has a substantial influence on transplantation related mortality, occurrence of graft-versus-host disease and relapse of diseases. For example, high numbers of infused $CD34^+$ $CD19^+$ B progenitors were associated with lower incidences of acute GVHD and transplant related mortality [23]. More information about stages of B lymphopoiesis and how they vary in different stem cell sources could improve clinical outcomes.

We have now found that human $CD34^+$ cells from CB, BM and G-PB express a wide range of CD10 densities. Increasing levels of CD10 corresponded to expression of lymphoid related

transcription factors and markers, as well as loss of proliferative potential in two recently developed culture systems. Moreover, myeloid differentiation potential was not completely lost until CD10 levels were very high. Complete restriction to a B lineage lymphoid fate may be a very late event in human lymphopoiesis.

Results and Discussion

Hematopoietic progenitors in different sites vary with respect to CD10 density and composition

We developed a new co-culture system where $CD34^+$ hematopoietic cells are sorted and placed on monolayers of human mesenchymal stem cells along with stem cell factor (SCF) and Flt3 ligand (see Materials & Methods). Under these conditions, $CD10^+$ $CD19^+$ lymphocytes emerged within 2–3 weeks. As noted in previous studies, the source of the progenitors was an important variable, and the efficiency was reproducibly higher in cultures initiated with CB (Figure S1) [13,24,25]. Differences in the composition of $CD34^+$ cell suspensions might account for this, because it has been found that $CD10^+$ progenitors from CB and BM are functionally equivalent [14,26]. That is, we considered that CB could be enriched with respect to $CD10^+$ CLP. To our surprise, BM contained more $CD10^+$ cells, and the average density of this marker was much higher (Figure 1).

$CD34^+$ cells were then enriched in samples representing three sources and flow cytometry was used to discern expression of other markers associated with early events in human hematopoiesis (Figure 2). Down-regulation of CD117/c-Kit occurs with progression from the stem/multipotential progenitor stage, and this receptor for SCF was entirely lacking in the $CD10^{Hi}$ subset of $CD34^+$ cells. Similarly, the CD135 receptor for Flt3 ligand, the CD90/Thy-1 antigen and the CD123 receptor for interleukin 3 were low on $CD10^{Hi}$ cells. Only small numbers of $CD10^{Lo}$ cells in BM displayed the CD33 myeloid marker. The deficiency of stem and early progenitor markers was offset by expression of CD9, CD24 and CD19 lymphoid associated antigens on $CD10^{Hi}$ $CD34^+$ cells. Although the incidence of $CD10^+$ cells in G-PB was low, staining patterns with the other markers were very similar to CB and BM (data not shown). In fact, when $CD34^+$ cells were resolved according to CD10 density, patterns of all other markers were remarkably similar, regardless of tissue of origin. As is the case with murine studies, there is no standardized definition of human CLP, and a series of markers have been used to resolve lymphopoietic progenitors. $CD34^+$ progenitors with low CD10 most closely resemble the original CLP described by Galy and colleagues [11]. CD24 was absent from $CD34^+$ $CD10^{Lo}$ progenitors suggesting they are not dedicated to the B lineage [16].

To obtain more detailed information about B lineage progression, we studied CD22, CD20 and cytoplasmic Igμ (cIgμ) expression with each of the three subsets (Figure 3A, B). Approximately, 20% of $CD34^+$ $CD10^{Hi}$ cells expressed CD22, and 5–10% of them were $CD20^+$. There were very few cIgμ positive cells among CB and BM $CD34^+$ fraction (less than 2% of $CD34^+$ cells). Zelm et al. reported that incomplete D_H-J_H rearrangements were initiated in $CD34^+$ $CD22^+CD19^-$ cells, and V_H-DJ_H rearrangements mainly occurred in $CD34^-$ $CD10^+$ $CD19^+$ $CD20^-$ cells [27]. *IgK/IgL* gene rearrangements were initiated after CD34 down-regulation and expression of cIgμ (in $CD34^-$ $CD10^+$ $CD19^+$ $CD20^-$ cells). Therefore, we analyzed immunoglobulin D_H-J_H gene rearrangements by quantitative PCR in subsets separated on the basis of CD10. The human IgH locus contains 66 rearrangeable V_H, 27 D_H, and 6 J_H genes, so we designed probes to detect the predominant D_H3–10 gene segment and the J_H4 gene segment. This particular D_H-J_H rearrangement

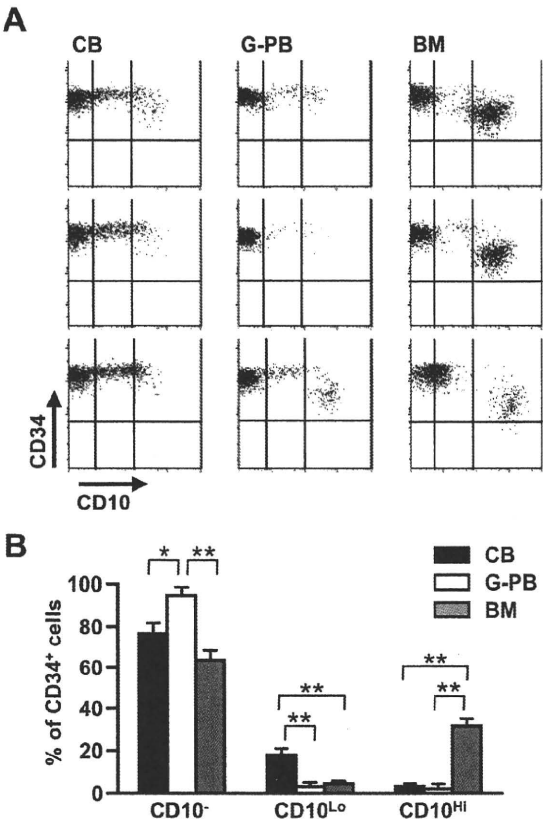

Figure 1. Densities of CD10 vary among human $CD34^+$ cells isolated in different ways. $CD34^+$ cells enriched from CB, G-CSF mobilized peripheral blood (G-PB) and BM were stained with PE-CD10 and APC-CD34 for flow cytometry analysis. (A) They were partitioned into three categories according to CD10 levels. (B) Incidences of $CD34^+$ $CD10^-$, $CD34^+$ $CD10^{Lo}$, and $CD34^+$ $CD10^{Hi}$ progenitors in these preparations are shown. Similar results were obtained in three independent experiments utilizing specimens from four different donors. Statistical significances were determined by unpaired two-tailed *t* test analysis: *, $p<0.05$ and **, $p<0.01$.
doi:10.1371/journal.pone.0012954.g001

most frequently occurs in humans [28]. Contrary to our expectations, Ig gene rearrangement was a late event, with high levels found only in the $CD34^+$ $CD10^{Hi}$ subset. Similar results were obtained in three independent experiments using cord blood or adult marrow derived progenitors.

Hematopoietic cells in humans and mice differ with respect to many cell surface markers [1–7,11–16,27,29], complicating extrapolation between the two (Figure S2). For example, freshly isolated murine lymphoid progenitors do not express CD10 [10]. In contrast, we now show that levels parallel lineage progression in humans. Our results suggest that CD10 levels represent an important variable, increasing coincident with initiation of Ig gene rearrangement and before uniform expression of either CD20 or CD22. Subsequent experiments were aimed at determining if it corresponded to differentiation and lineage restriction.

CD10 density increases with expression of lymphoid lineage transcription factors, but loss of myeloid potential by CD10 bearing progenitors is a late event

Consistent with changes in proteins detected by flow cytometry, transcripts for the RAG-1recombinase enzyme markedly increased

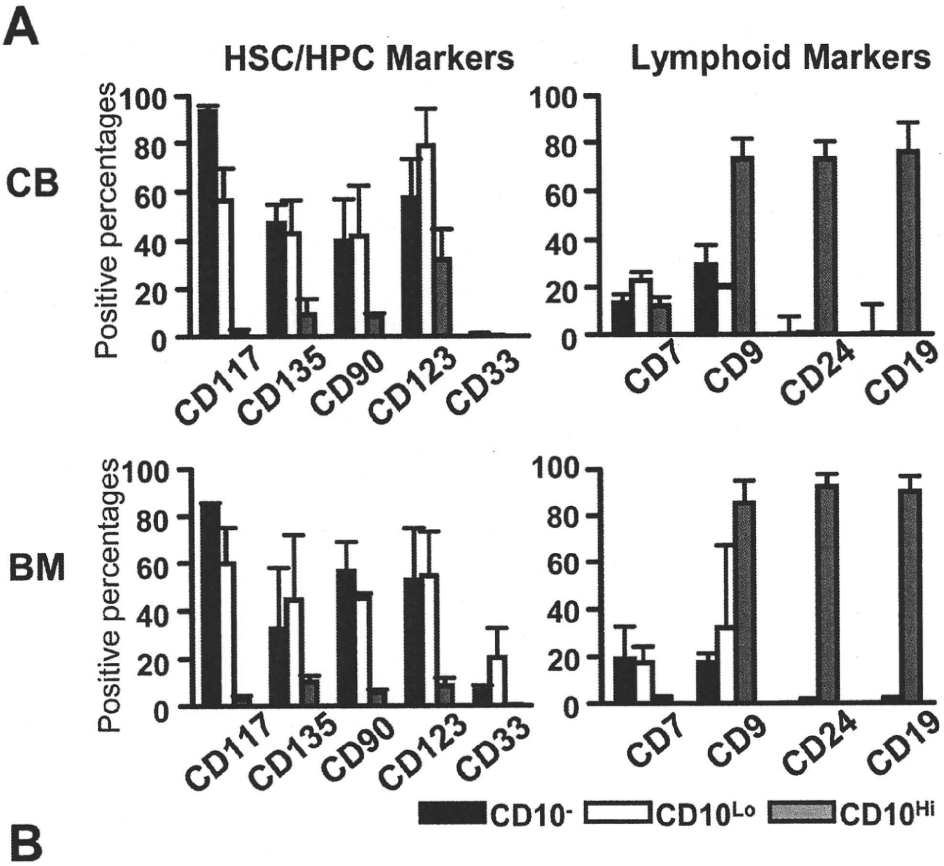
A
HSC/HPC Markers
Lymphoid Markers
CB
BM
Positive percentages
100
80
60
40
20
0
CD117
CD135
CD90
CD123
CD33
CD7
CD9
CD24
CD19
CD10-
CD10Lo
CD10Hi

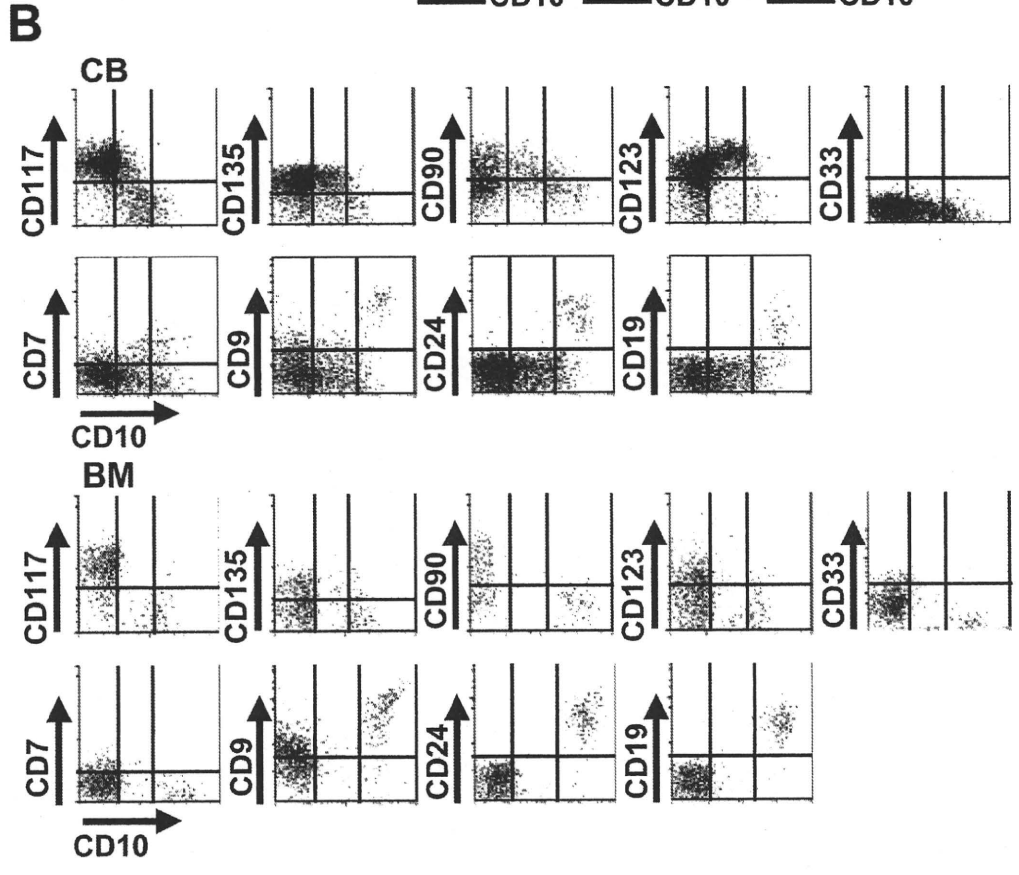
B
CB
BM
CD117
CD135
CD90
CD123
CD33
CD7
CD9
CD24
CD19
CD10

Figure 2. High levels of CD10 correspond to progression in the B lineage. (A, B) CD34$^+$ cells from CB and BM were stained with CD10 and CD34 as well as the indicated antibodies, and analyzed by flow cytometry. The CD34$^+$ cells were gated according to CD10 levels and percentages of cells positive for each marker are shown. Similar results were obtained with cells from at least three different donors in three separate experiments.
doi:10.1371/journal.pone.0012954.g002

with CD10 up-regulation (Figure 4). The Ebf1 and Pax5 transcription factors are essential for B lymphopoiesis, and the corresponding transcripts increased in parallel with CD10. In contrast, expression of the myeloid associated myeloperoxidase (MPO) gene was down-regulated with CD10 acquisition. All of these three subsets expressed C/Ebpα and Notch1. Results were very similar when CB rather than BM was used as a source of progenitors (data not shown). Hystad and colleagues performed microarray analyses on human B lineage progenitors separated according to presence or absence of markers [29]. Comparing their developmental milestones to our RT-PCR results indicates that CD34$^+$ CD10^{Lo} cells are relatively primitive, but primed for lymphopoiesis. Abrupt increases in CD10 transcripts were found in another study to correspond with Ig gene rearrangement activity [27].

Interestingly, the experiments described above revealed that CD34$^+$ progenitors with CD10 still had C/Ebpα gene expression, and CD34$^+$ CD10^{Lo} progenitors expressed MPO at a low level, as reported before [27,29]. This raises important questions concerning their differentiation potential. Therefore, we sorted CD34$^+$ cells from CB and carefully assessed their progeny over four weeks of culture (Figure 5A, B). A substantial wave of CD33$^+$ myeloid cells was observed in cultures initiated with CD34$^+$ CD10^{Lo} progenitors,

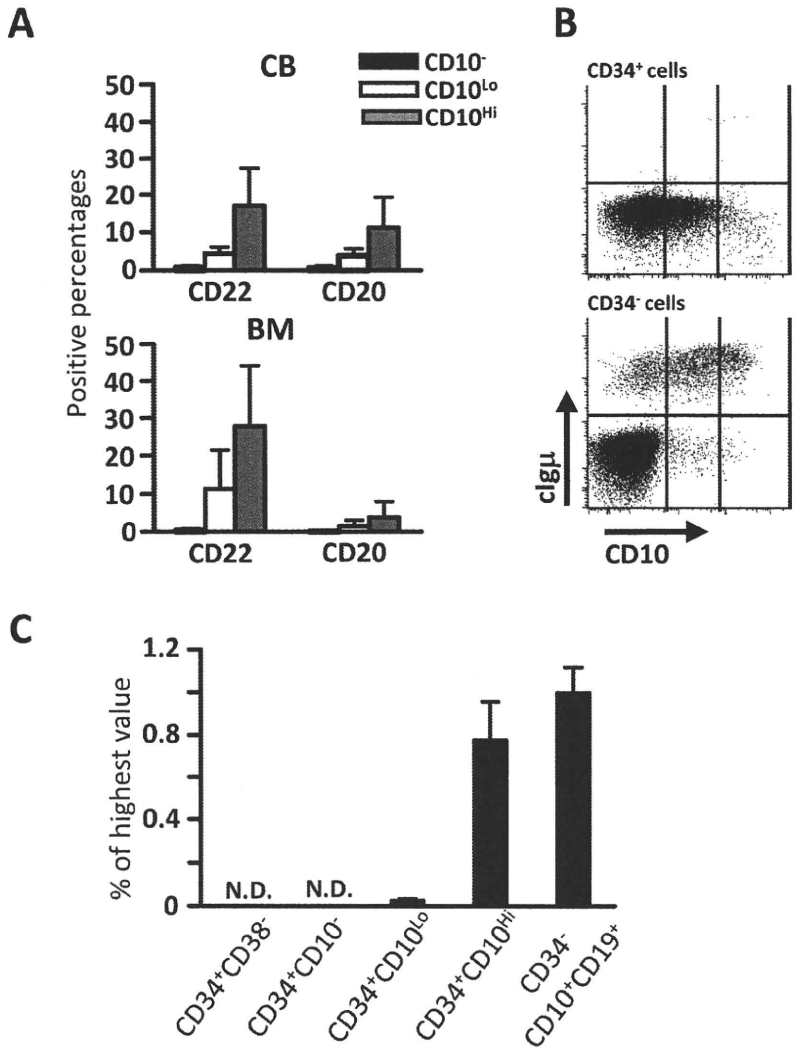

Figure 3. D_H-J_H rearrangements\cur in progenitors with high CD10 densities. (A) Expression patterns of CD22 and CD20 on CD34$^+$ CD10$^-$, CD34$^+$ CD10^{Lo}, and CD34$^+$ CD10^{Hi} progenitors derived from CB and BM were analyzed using flow cytometry. (B) After staining CD34$^+$ or CD34$^-$cells from CB and BM with CD10 and CD34 antibodies and fixing, they were stained with cytoplasmic Igμ. The data is representative of results obtained with cells from at least three diffferent donors in three separate experiments. (C) The indicated fractions were sorted from CB, and genomic DNA was extracted from 10^4 cells. Sorted CD34$^+$ CD38$^-$ and CD34$^-$ CD10$^+$ CD19$^+$ cells were used as negative and positive controls, respectively. C/Ebpα specific PCR reactions were used to determine input quantities. The results are normalized as percentages of peak values for each of the genes and are representative of that obtained in three independent experiments, using either CB or BM. N.D.; not detected.
doi:10.1371/journal.pone.0012954.g003

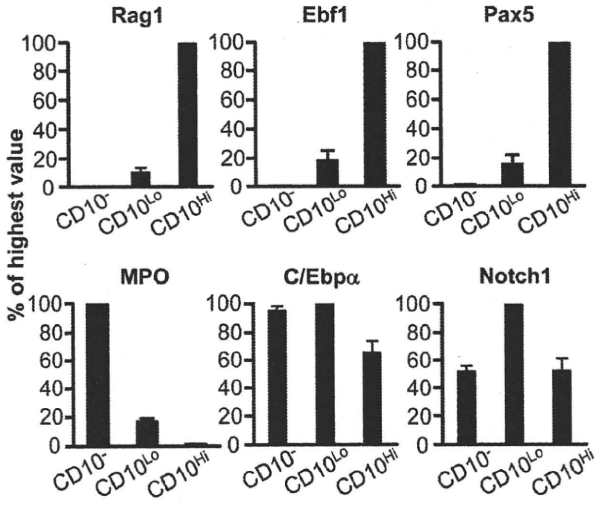

Figure 4. Gene expression patterns suggest that lymphoid commitment parallels acquisition of CD10. $CD34^+$ $CD10^-$, $CD34^+$ $CD10^{Lo}$ and $CD34^+$ $CD10^{Hi}$ cells were sorted from BM. mRNA was extracted from each subset, and quantitative RT-PCR was conducted. The results are normalized as percentages of peak values for each of the genes and are representative of three independent experiments. Similar results were obtained in three experiments, using either CB or BM.
doi:10.1371/journal.pone.0012954.g004

and sustained myelopoiesis resulted in remaining cultures of $CD10^-$ stem/progenitors. Human mesenchymal stromal cells were used for these experiments because of their ability to simultaneously support B, dendritic and myeloid differentiation. Therefore, we recovered $CD14^-$ $CD19^-$ $CD11c^+$ $CD123^{Lo/-}$ conventional dendritic cells, as well as $CD14^-$ $CD19^-$ $CD11c^-$ $CD123^{Hi}$ plasmacytoid dendritic cells from 2 week co-cultures (Figure 5C, D). We conclude that $CD10^{Lo}$ progenitors are not lymphoid lineage restricted.

$CD34^+$ $CD10^{Hi}$ progenitors are strictly lineage-committed, but have diminished ability to expand in culture

Given that $CD10^{Hi}$ progenitors express characteristics associated with B lineage lymphocytes, we assumed that they would be potent progenitors when placed in culture. However, yields of total cells and $CD19^+$ B lineage lymphocytes were very low at all time points in cultures initiated with $CD34^+$ $CD10^{Hi}$ progenitors (Figure 5, 6A). This is despite the fact that these culture conditions are optimized for human B lymphopoiesis [30] and gave good yields with $CD10^-$ and $CD10^{Lo}$ subsets (Figure 5, 6A). Late stages of murine B lymphopoiesis are most efficiently supported by stromal cell-free conditions [31], and we recently adapted that approach for human progenitors [32]. However, attempts to propagate them in four-week stromal cell-free cultures were unsuccessful (Figure 6B).

In one-week stromal cell-free cultures, $CD34^+$ $CD10^{Hi}$ progenitors gave rise to $CD34^-$ $CD33^-$ $CD19^+$ lymphocytes, but only with poor survival and/or minimal expansion (Figure 6C). In contrast to $CD34^+$ $CD10^-$ and $CD34^+$ $CD10^{Lo}$ progenitors, the $CD10^{Hi}$ subset proliferated poorly during four days of culture and incorporated little BrdU (Figure 6D). This contrasts with a report that some $CD34^+CD19^+$ cells could generate myeloid and erythroid lineage cells [33]. Although $CD10^{Hi}$ progenitors are rare in CB, we were able to determine that they also expanded poorly in these cultures.

It is possible that $CD34^+$ $CD10^{Hi}$ progenitors are post-mitotic *in vivo*, but staining of freshly isolated BM with the Ki67 proliferation marker revealed that all three subsets include dividing cells (Figure 7A, B). The restricted and rapid generation of $CD34^-$ $CD19^+$ lymphocytes by $CD34^+$ $CD10^{Hi}$ progenitors suggests they represent a lineage committed stage. They could have recently exited cell cycle in vivo. Alternatively, conditions required for their expansion in culture remain undefined.

Definition of factors that regulate human B lymphopoiesis remains an elusive goal, and no cytokine that supports robust human B lymphopoiesis has been found. B lymphopoiesis is not impaired in SCID patients with mutations in the common γ chain required for IL-7 responses, and there is no clear requirement for this cytokine in cultures of freshly isolated progenitors [19,30,32,34–36]. On the other hand, there is some evidence that stromal cells and pre-cultured hematopoietic cells can recognize IL-7 [37–40]. In addition, a very transient response of human fetal B progenitor cells was reported [19,41,42].

To conclude, the composition of umbilical cord blood, G-CSF mobilized peripheral blood and adult bone marrow is markedly different with respect to lymphopoietic cell subsets. Our results show that CD10 density increases in parallel with expression of B lymphoid lineage genes and surface markers on $CD34^+$ progenitors. This parameter also corresponds to loss of potential to generate myeloid and dendritic cells in culture. Complete restriction to a B lineage fate appears to be a late event.

Materials and Methods

Origin and isolation of cells

CB cells were collected from healthy, full-term neonates immediately after Caesarean section or normal delivery. BM and G-CSF mobilized PB cells were collected from normal healthy donors. All samples were collected after written informed consent, using protocols approved by the Investigational Review Boards at Osaka University and Oklahoma Medical Research Foundation. Mononuclear cells were separated by Ficoll-Paque PLUS (GE Healthcare Bio-Science AB, Uppsala, Sweden) or Lymphocyte Separation Medium (Mediatech, Inc., Manassas, VA) and centrifugation. Purification of CB and BM $CD34^+$ cells was performed using Direct human CD34 Progenitor Cell Isolation Kit (Miltenyi Biotec, Auburn, CA). Human specimens were separately analyzed with respect to progenitor phenotypes to reveal individual to individual variability. Rare progenitor cells were mixed to have sufficient numbers to initiate culture experiments. Human mesenchymal stem cells were purchased from Lonza (Walkersville, MD), and maintained in Mesenchymal Stem Cell Growth Medium (MSCGM, Lonza). Flow cytometric analysis confirmed that the cultured hMSC expressed CD105, CD166, CD29, and CD44, but not CD14, CD34, or CD45.

Co-cultures for human B lymphocytes

Co-cultures of $CD34^+$ cells on hMSC were performed as previously described [30]. hMSC were seeded in 12-well tissue plates 1 or 2 days before setting up the co-cultures. Isolated $CD34^+$ cells (2×10^3 cells/well) were plated on sub-confluent hMSC layers in MSCGM in the presence of 10 ng/ml SCF and 5 ng/ml FL. Recombinant human SCF and FL proteins were purchased from R&D Systems, Inc. (Minneapolis, MN). Half of the culture medium was replaced with fresh medium containing the same cytokines twice a week.

Stromal cell-free cultures for human B lymphocytes

Stromal cell-free cultures were performed as previously described [32]. The cultures were usually maintained in QBSF®60 (Quality Biological, Inc., Gaithersburg, MD) containing10% FCS, 100 U/ml penicillin, and 100 mg/ml streptomycin with indicated cytokines.

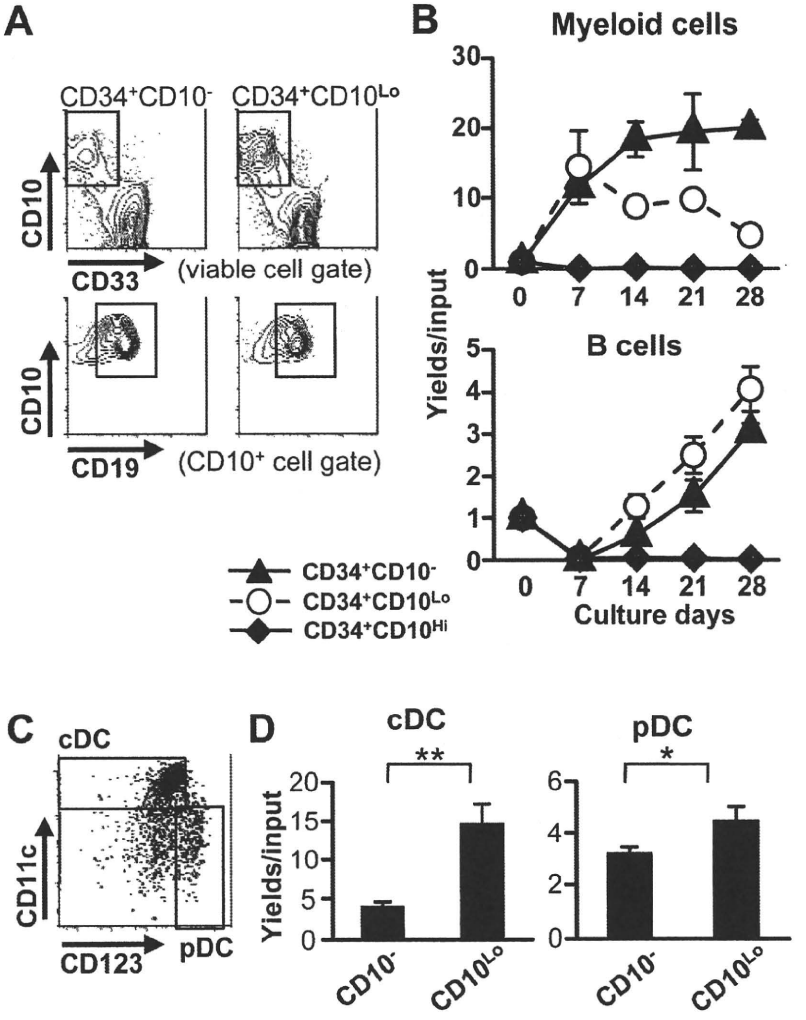

Figure 5. Both CD34$^+$ CD10$^-$ and CD34$^+$ CD10^{Lo} subsets can generate DC and myeloid lineage cells. (A, B) CD34$^+$ CD10$^-$, CD34$^+$ CD10^{Lo} and CD34$^+$ CD10^{Hi} cells were sorted from CB and cultured with hMSC in the presence of SCF and FL for 4 weeks. Representative flow cytometry results are shown for a 4 week co-culture experiment performed with pooled cord blood specimens (A). The cultured cells were collected weekly, and numbers of generated CD33$^+$ myeloid cells (B, upper panel) and CD10$^+$ CD19$^+$ B cells (B, lower panel) were determined. Similar results were obtained in three independent experiments. (C, D) CD34$^+$ CD10$^-$ and CD34$^+$ CD10^{Lo} CB cells were cultured with hMSC in the presence of SCF and FL for 2 weeks. Cells recovered and gated as CD14$^-$, CD34$^-$ and CD19$^-$ were characterized by flow cytometry (C), and numbers used to calculate yields per input cells (D). Similar results were obtained in three independent experiments. Statistical significances were determined by unpaired two-tailed *t* test analysis: *, $p<0.05$ and **, $p<0.01$.
doi:10.1371/journal.pone.0012954.g005

Recombinant human IL-7 and G-CSF proteins were purchased from R&D Systems. Half of the culture medium was replaced with fresh medium containing the same cytokines once a week. The cytokines were used at the following concentrations: SCF, 10 ng/ml; FL, 5 ng/ml; G-CSF, 10 ng/ml; and IL-7, 5 ng/ml.

Flow cytometry and cell sorting

Flow cytometric analysis was performed with a FACS Calibur or FACS LSRII (BD Biosciences Immunocytometry Systems, San Jose, CA) using standard multicolor immunofluorescent staining protocols. Mouse monoclonal Abs against the following human cell surface molecules were purchased: phycoerythrin (PE)-CD7, FITC-CD9, PE-CD10, allophycocyanin (APC)-CD10, APC-CD11c, FITC-CD14, PE-CD19, FITC-CD20, FITC-CD33, PE-CD34, APC-CD34, APC-CD90, PE-CD117, PE-CD123, PE-CD135, FITC-IgM and FITC-Ki67 from BD Bioscieinces/BD Pharmingen (Franklin Lakes, NJ); APC-CD22 from Bio Legend (San Diego, CA); phycoerythrin 5-succinimidylester (PC5)-CD19, PC5-CD24 from Beckman Coulter (Marseilles, France). In some experiments, CD34$^+$ CD10$^-$, CD34$^+$ CD10^{Lo} and CD34$^+$ CD10^{Hi} cells were sorted using a FACS Aria (BD Biosciences Immunocytometry Systems) and subjected to the cultures for human B lymphocytes. In this case, enriched CD34$^+$ cells were stained with APC-CD34 and PE-CD10.

Real-time quantitative PCR analysis of IgH gene rearrangement

A Genomic DNA was isolated from 1×10^4 sorted subsets with a DNeasy Tissue Kit (QIAGEN, Valencia, CA). Taqman-based quantitative PCR was used to detect IgH gene rearrangement, using TaqMan Universal PCR Master Mix (Applied Biosystems, Foster City, CA). The probe was designed to detect one of the

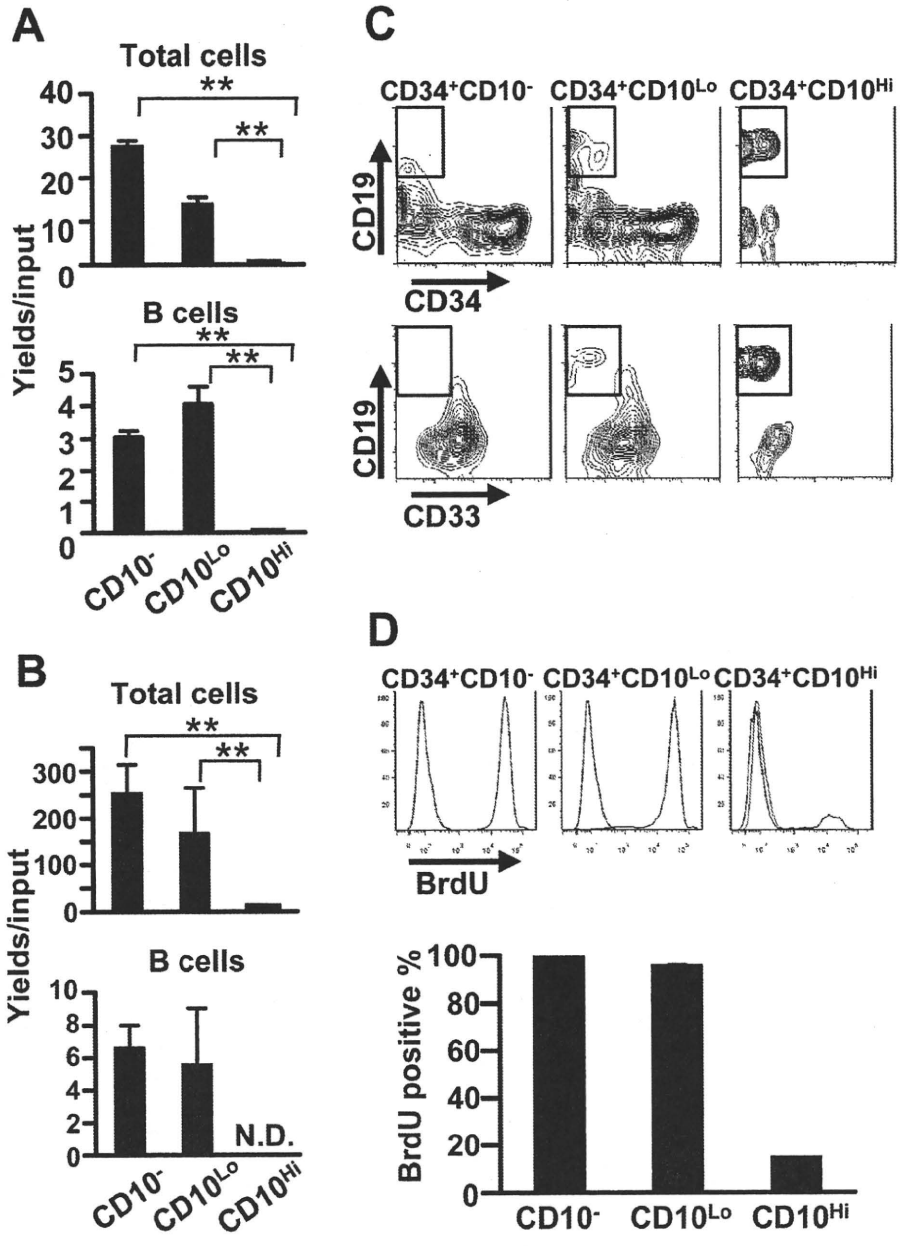

Figure 6. CD34$^+$ CD10^{Hi} progenitors can differentiate but not proliferate in vitro. (A) CD34$^+$ CD10$^-$, CD34$^+$ CD10^{Lo} and CD34$^+$ CD10^{Hi} cells were sorted from CB and stromal cell co-cultures were maintained with SCF and FL for 4 weeks before flow cytometry analyses. (B) The three categories of CD34$^+$ CB progenitors were cultured under stromal cell-free conditions, but with SCF, FL and IL-7 for 3 weeks. Numbers of total and CD10$^+$ CD19$^+$ cells per input progenitor were calculated. (C) CD34$^+$ CD10^{Lo} and CD34$^+$ CD10^{Hi} cells were sorted from BM and cultured under stromal cell-free conditions for 1 week. The generated cells were stained with CD19, CD33 and CD34 and were analyzed by flow cytometry. One representative determination is shown. (D) CD34$^+$ CD10$^-$, CD34$^+$ CD10^{Lo} and CD34$^+$ CD10^{Hi} cells were sorted from CB and cultured in the presence of SCF, FL, and G-CSF for 4 days. They were pulsed with 10 mM BrdU for the final 48 hours. Similar results were obtained in three independent experiments. Statistical significances were determined by unpaired two-tailed *t* test analysis: **, $p<0.01$. N.D.; not detected.
doi:10.1371/journal.pone.0012954.g006

main D_H gene segment families (D_H3–10) and J_H4 gene segment, where D_H-J_H rearrangement most frequently occurrs in humans (Applied Biosystems) [28]. Expression levels were determined by the internal control gene (C/Ebpα). Each sample was measured in triplicate, and the comparative threshold cycle method was used for relative quantification of gene expression. The primer sequences are available from the authors on request.

RNA isolation and Real-time quantitative PCR analysis of gene expression

The mRNAs were isolated from sorted cells by using RNeasy Mini Kit (QIAGEN). The cDNAs were then prepared from DNase I-treated mRNA by using oligo(dT) and Moloney murine leukemia virus reverse transcriptase (Invitrogen, Carlsbad, CA). Reactions were quantified with fluorescent TaqMan technology.

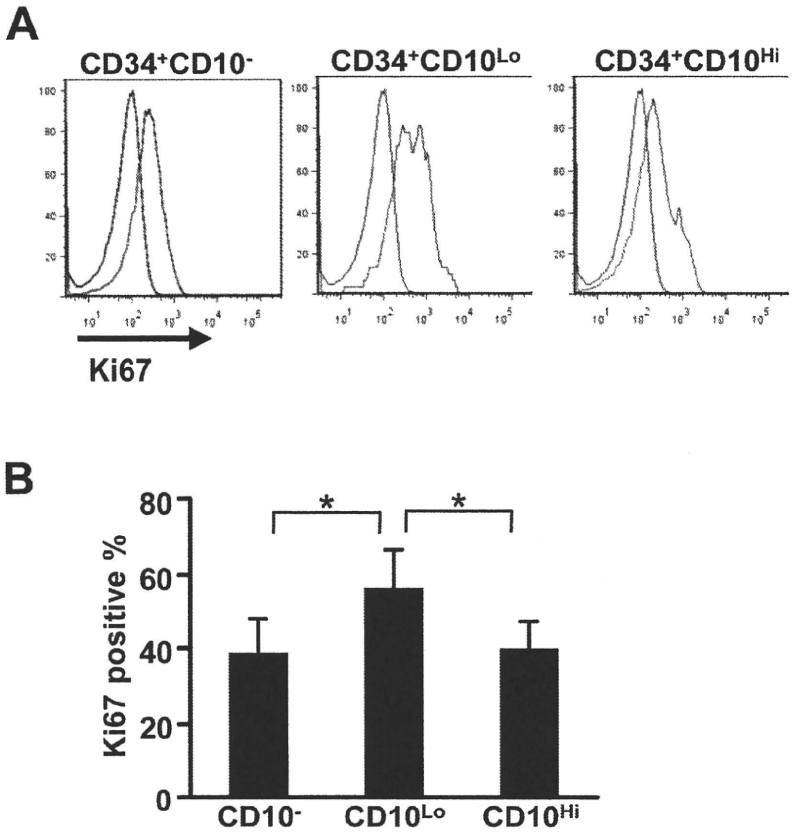

Figure 7. All three subsets include dividing cells when freshly isolated from BM. $CD34^+$ $CD10^-$, $CD34^+$ $CD10^{Lo}$ and $CD34^+$ $CD10^{Hi}$ cells were sorted from fresh BM, and Ki67 expression was analyzed on the three subsets. A representative analysis is shown (A) and the data represent mean values with standard deviations from 6 samples (B). Statistical significances were determined by unpaired two-tailed *t* test analysis: *, $p<0.05$.
doi:10.1371/journal.pone.0012954.g007

TaqMan primers and probes specific for indicated or S18 gene were used in the ABI750 sequence detection system (Applied Biosystems). Reactions were run at an annealing temperature of 60°C with 40 cycles. Each sample was measured in triplicate, and the comparative threshold cycle method was used for relative quantification of gene expression.

BrdU assay

$CD34^+$ $CD10^-$, $CD34^+$ $CD10^{Lo}$ and $CD34^+$ $CD10^{Hi}$ cells were sorted and cultured in the presence of 10 ng/ml SCF, 5 ng/ml FL, and 10 ng/ml G-CSF for 4 days. They were pulsed with 10 mM BrdU for the final 48 hours. FITC BrdU Flow Kit purchased from BD Bioscieinces/BD Pharmingen was used.

Statistical analyses

Student's t-test was performed to assess statistical differences. All results are shown as mean values ± SD.

Supporting Information

Figure S1 The efficiency of B cell generation in culture depends on the source of progenitor cells. $CD34^+$ cells were sorted from CB, G-CSF mobilized peripheral blood (G-PB) or BM, and cultured with hMSC in the presence of SCF and FL for 4 weeks. A representative analysis is shown (A). Numbers of total and $CD10^+$ $CD19^+$ B cells generated were calculated (B). Similar results were obtained in three independent experiments. Statistical significances were determined by unpaired two-tailed t test analysis: *, $p<0.05$ and **, $p<0.01$.
Found at: doi:10.1371/journal.pone.0012954.s001 (0.45 MB TIF)

Figure S2 Comparison of B lymphopoiesis in mice and humans. Our new results and ones from the literature were used to construct a possible sequence of events in human B lymphocyte formation. Progressive down-regulation of c-Kit occurs from stem/early progenitor stages in mice, and our observations suggest that is also the case for humans. Three categories of human $CD10^-$, $CD10^{Lo}$ and $CD10^{Hi}$ cells evaluated in the present study are positioned with respect to stem cells and lymphoid committed progenitors.
Found at: doi:10.1371/journal.pone.0012954.s002 (0.25 MB TIF)

Acknowledgments

We thank Shelli Wasson for editorial assistance, Jacob Bass and Dr. Diana Hamilton for cell sorting, and Beverly Hurt for graphics support.

Author Contributions

Conceived and designed the experiments: MI KO TY QZ KPG PWK. Performed the experiments: MI. Analyzed the data: MI PWK. Contributed reagents/materials/analysis tools: MI KO YK PWK. Wrote the paper: MI KO TY KPG YK PWK.

References

1. Kondo M, Weissman IL, Akashi K (1997) Identification of clonogenic common lymphoid progenitors in mouse bone marrow. Cell 91: 661–672.
2. Harman BC, Northrup DL, Allman D (2008) Resolution of unique Sca-1^{high}c-Kit^{+} lymphoid-biased progenitors in adult bone marrow. J Immunol 181: 7514–7524.
3. Rumfelt LL, Zhou Y, Rowley BM, Shinton SA, Hardy RR (2006) Lineage specification and plasticity in CD19^{-} early B cell precursors. J Exp Med 203: 675–687.
4. Kawamoto H, Katsura Y (2009) A new paradigm for hematopoietic cell lineages: revision of the classical concept of the myeloid-lymphoid dichotomy. Trends Immunol 30: 193–200.
5. Balciunaite G, Ceredig R, Massa S, Rolink AG (2005) A B220^{+} CD117^{+} CD19^{-} hematopoietic progenitor with potent lymphoid and myeloid developmental potential. Eur J Immunol 35: 2019–2030.
6. Karsunky H, Inlay MA, Serwold T, Bhattacharya D, Weissman IL (2008) Flk2^{+} common lymphoid progenitors possess equivalent differentiation potential for the B and T lineages. Blood 111: 5562–5570.
7. Inlay MA, Bhattacharya D, Sahoo D, Serwold T, Seita J, et al. (2009) Ly6d marks the earliest stage of B-cell specification and identifies the branchpoint between B-cell and T-cell development. Genes Dev 23: 2376–2381.
8. Hu M, Krause D, Greaves M, Sharkis S, Dexter M, et al. (1997) Multilineage gene expression precedes commitment in the hemopoietic system. Genes Dev 11: 774–785.
9. Welner RS, Pelayo R, Nagai Y, Garrett KP, Wuest TR, et al. (2008) Lymphoid precursors are directed to produce dendritic cells as a result of TLR9 ligation during herpes infection. Blood 112: 3753–3761.
10. Kee BL, Paige CJ, Letarte M (1992) Characterization of murine CD10, an endopeptidase expressed on bone marrow adherent cells. Int Immunol 4: 1041–1047.
11. Galy A, Travis M, Cen D, Chen B (1995) Human T, B, natural killer, and dendritic cells arise from a common bone marrow progenitor cell subset. Immunity 3: 459–473.
12. Crooks GM (2004) Common lymphoid progenitors. In:Handbook of Stem Cells Lanza R, Blau H, Melton D, Moore M, Thomas ED, et al. eds. pp 347–353, Elsevier, Inc., Burlington, MA.
13. Hao QL, Zhu J, Price MA, Payne KJ, Barsky LW, et al. (2001) Identification of a novel, human multilymphoid progenitor in cord blood. Blood 97: 3683–3690.
14. Haddad R, Guardiola P, Izac B, Thibault C, Radich J, et al. (2004) Molecular characterization of early human T/NK and B-lymphoid progenitor cells in umbilical cord blood. Blood 104: 3918–3926.
15. Hoebeke I, De SM, Stolz F, Pike-Overzet K, Staal FJ, et al. (2007) T-, B- and NK-lymphoid, but not myeloid cells arise from human CD34^{+}CD38^{-}CD7^{+} common lymphoid progenitors expressing lymphoid-specific genes. Leukemia 21: 311–319.
16. Six EM, Bonhomme D, Monteiro M, Beldjord K, Jurkowska M, et al. (2007) A human postnatal lymphoid progenitor capable of circulating and seeding the thymus. J Exp Med 204: 3085–3093.
17. Sanz E, Alvarez-Mon M, Martinez-AC, de la Hera A (2003) Human cord blood CD34^{+}Pax-5^{+} B-cell progenitors: single-cell analyses of their gene expression profiles. Blood 101: 3424–3430.
18. Sanz E, Munoz-AN, Monserrat J, Van-Den-Rym A, Escoll P, et al. (2010) Ordering human CD34^{+}CD10^{-}CD19^{+} pre/pro-B-cell and CD19^{-} common lymphoid progenitor stages in two pro-B-cell development pathways. Proc Natl Acad Sci USA 107: 5925–5930.
19. Pribyl JAR, Lebien TW (1996) Interleukin 7 independent development of human B cells. Proc Natl Acad Sci USA 93: 10348–10353.
20. Schmitz N, Barrett J (2002) Optimizing engraftment—source and dose of stem cells. Semin Hematol 39: 3–14.
21. Laughlin MJ, Eapen M, Rubinstein P, Wagner JE, Zhang MJ, et al. (2004) Outcomes after transplantation of cord blood or bone marrow from unrelated donors in adults with leukemia. N Engl J Med 351: 2265–2275.
22. Tomblyn MB, Arora M, Baker KS, Blazar BR, Brunstein CG, et al. (2009) Myeloablative hematopoietic cell transplantation for acute lymphoblastic leukemia: analysis of graft sources and long-term outcome. J Clin Oncol 27: 3634–3641.
23. Michonneau D, Peffault de LR, Porcher R, Robin M, Benbunan M, et al. (2009) Influence of bone marrow graft B lymphocyte subsets on outcome after HLA-identical sibling transplants. Br J Haematol 145: 107–114.
24. Wang JCY, Doedens M, Dick JE (1997) Primitive human hematopoietic cells are enriched in cord blood compared with adult bone marrow or mobilized peripheral blood as measured by the quantitative in vivo SCID-repopulating cell assay. Blood 89: 3919–3924.
25. Ng YY, van Kessel B, Lokhorst HM, Baert MR, van den Burg CM, et al. (2004) Gene-expression profiling of CD34^{+} cells from various hematopoietic stem-cell sources reveals functional differences in stem-cell activity. J Leukoc Biol 75: 314–323.
26. Rossi MID, Yokota T, Medina KL, Garrett KP, Comp PC, et al. (2003) B lymphopoiesis is active throughout human life, but there are developmental age related changes. Blood 101: 576–584.
27. van Zelm MC, van der BM, de RD, Barendregt BH, de Haas EF, et al. (2005) Ig gene rearrangement steps are initiated in early human precursor B cell subsets and correlate with specific transcription factor expression. J Immunol 175: 5912–5922.
28. Lefranc MP, Clement O, Kaas Q, Duprat E, Chastellan P, et al. (2005) IMGT-Choreography for immunogenetics and immunoinformatics. In Silico Biol 5: 45–60.
29. Hystad ME, Myklebust JH, Bo TH, Sivertsen EA, Rian E, et al. (2007) Characterization of early stages of human B cell development by gene expression profiling. J Immunol 179: 3662–3671.
30. Ichii M, Oritani K, Yokota T, Nishida M, Takahashi I, et al. (2008) Regulation of human B lymphopoiesis by the transforming growth factor-β superfamily in a newly established coculture system using human mesenchymal stem cells as a supportive microenvironment. Exp Hematol 36: 587–597.
31. Kouro T, Medina KL, Oritani K, Kincade PW (2001) Characteristics of early murine B lymphocyte precursors and their direct sensitivity to negative regulators. Blood 97: 2708–2715.
32. Ichii M, Oritani K, Yokota T, Holter JL, Schultz DC, et al. (2010) Stromal cell-free conditions favorable for human B lymphopoiesis in culture. J Immunol Methods 359: 47–55.
33. Hou YH, Srour EF, Ramsey H, Dahl R, Broxmeyer HE, et al. (2005) Identification of a human B-cell/myeloid common progenitor by the absence of CXCR4. Blood 105: 3488–3492.
34. Buckley RH (2010) B-cell function in severe combined immunodeficiency after stem cell or gene therapy: a review. J Allergy Clin Immunol 125: 790–797.
35. Buckley RH (2004) Molecular defects in human severe combined immunodeficiency and approaches to immune reconstitution. Annu Rev Immunol 22: 625–655.
36. Nishihara M, Wada Y, Ogami K, Ebihara Y, Ishii T, et al. (1998) A combination of stem cell factor and granulocyte colony-stimulating factor enhances the growth of human progenitor B cells supported by murine stromal cell line MS-5. Eur J Immunol 28: 855–864.
37. Johnson SE, Shah N, Panoskaltsis-Mortari A, Lebien TW (2005) Murine and human IL-7 activate STAT5 and induce proliferation of normal human pro-B cells. J Immunol 175: 7325–7331.
38. Johnson SE, Shah N, Bajer AA, Lebien TW (2008) IL-7 activates the phosphatidylinositol 3-kinase/AKT pathway in normal human thymocytes but not normal human B cell precursors. J Immunol 180: 8109–8117.
39. Parrish YK, Baez I, Milford TA, Benitez A, Galloway N, et al. (2009) IL-7 Dependence in human B lymphopoiesis increases during progression of ontogeny from cord blood to bone marrow. J Immunol 182: 4255–4266.
40. Iwata M, Graf L, Awaya N, Torok-Storb B (2002) Functional interleukin-7 receptors (IL-7Rs) are expressed by marrow stromal cells: binding of IL-7 increases levels of IL-6 mRNA and secreted protein. Blood 100: 1318–1325.
41. Dittel BN, Lebien TW (1995) The growth response to IL-7 during normal human B cell ontogeny is restricted to B-lineage cells expressing CD34. J Immunol 154: 58–67.
42. Wolf ML, Buckley JA, Goldfarb A, Law C-L, Lebien TW (1991) Development of a bone marrow culture for maintenance and growth of normal human B cell precursors. J Immunol 147: 3324–3330.

Heart Vessels (2010) 25:444–447
DOI 10.1007/s00380-009-1215-5

CASE REPORT

Yoh Arita · Yasushi Sakata · Takao Sudo · Tetsuo Maeda
Ken Matsuoka · Keito Tamai · Kaori Higuchi
Wataru Shioyama · Yoshikazu Nakaoka
Yuzuru Kanakura · Keiko Yamauchi-Takihara

The efficacy of tocilizumab in a patient with pulmonary arterial hypertension associated with Castleman's disease

Received: April 3, 2009 / Accepted: October 16, 2009

Abstract Castleman's disease is a highly heterogeneous clinical–pathological entity that belongs to the lymphoproliferative disorders and is associated with pulmonary arterial hypertension (PAH) in some patients. It is linked to excessive immune stimulation by interleukin-6 (IL-6), which is also involved in the pathogenesis of PAH. A 31-year-old woman with Castleman's disease demonstrated PAH characterized by severe right heart failure. Since she was resistant to various conventional therapies including steroids, prostacyclins, bosentan, and sildenafil, tocilizumab (anti-IL-6 receptor antibody) therapy was started. Her clinical course was followed for 6 months, with significant improvement without any adverse effect. This is the first reported case of use of tocilizumab in addition to steroids and conventional PAH therapy in a patient with PAH associated with Castleman's disease.

Key words Pulmonary arterial hypertension · Interleukin-6 · Cytokine · Interleukin-6 receptor

Introduction

Castleman's disease is a rare clinical–pathological entity that belongs to the lymphoproliferative disorders, and is responsible for lymph node enlargement.[1,2] It can be classified into two forms: the hyaline vascular (localized) type and the plasma-cell (multicentric) type. In general, the localized form is asymptomatic or presents as an isolated enlarged lymph node, while multicentric Castleman's disease often results in diffuse lymphadenopathy, and is frequently associated with hepatosplenomegaly and various systemic manifestations.

Interleukin-6 (IL-6) plays crucial pathological roles in immune-inflammatory diseases such as rheumatoid arthritis and Castleman's disease,[3] and also in various cardiovascular diseases.[4] Recently, the humanized anti-IL-6 receptor (IL-6R) antibody, tocilizumab, has been widely used for the treatment of these inflammatory disorders.[5–7] Anti-IL-6R therapy is reported to improve clinical symptoms of Castleman's disease and to normalize acute-phase proteins, such as C-reactive protein (CRP) and serum amyloid A.[5]

Pulmonary arterial hypertension (PAH) is a rare progressive disease, characterized by elevated pulmonary arterial resistance[8] leading to right heart failure with poor prognosis. Pulmonary arterial hypertension can be sporadic, familial, or secondary to other conditions, including connective tissue disease, congenital systemic-to-pulmonary shunt, portal hypertension, human immunodeficiency virus (HIV) infection, and appetite suppressant exposure.[9] A total of three cases of PAH have been reported to occur in association with Castleman's disease in HIV-negative or -positive patients.[10,11] Here we report for the first time successful treatment of PAH associated with Castleman's disease using tocilizumab, in a patient who had been resistant to conventional therapy including steroids, prostacyclins, bosentan, and sildenafil.

Case report

A 31-year-old woman was admitted to a hospital with the complaint of dyspnea in 1995. She was clinically diagnosed with Castleman's disease by lymph node biopsy and was negative for HIV infection. She was started on steroid therapy (prednisolone 60 mg/day).

In October 2007, she gradually developed severe edema and New York Heart Association (NYHA) class III dyspnea. Her estimated right ventricular systolic pressure (RVSP) was 85 mmHg on echocardiography, and she was transferred to Osaka University Hospital in February 2008. On

Y. Arita · Y. Sakata · K. Matsuoka · K. Tamai · K. Higuchi · W. Shioyama · Y. Nakaoka · K. Yamauchi-Takihara (✉)
Department of Cardiovascular Medicine, Osaka University Graduate School of Medicine, 2-2 Yamadaoka, Suita, Osaka 565-0871, Japan
Tel. +81-6-6850-6012; Fax +81-6-6850-6040
e-mail: takihara@imed3.med.osaka-u.ac.jp

T. Sudo · T. Maeda · Y. Kanakura
Department of Hematology and Oncology, Osaka University Graduate School of Medicine, Osaka, Japan